

1 **Detailed Chemical Characterization of Unresolved Complex Mixtures (UCM) in**  
2 **Atmospheric Organics: Insights into Emission Sources, Atmospheric Processing and**  
3 **Secondary Organic Aerosol Formation**

4  
5 Arthur W. H. Chan<sup>1</sup>, Gabriel Isaacman<sup>1</sup>, Kevin R. Wilson<sup>2</sup>, David R. Worton<sup>1,3</sup>, Chris R. Ruehl<sup>1</sup>,  
6 Theodora Nah<sup>4</sup>, Drew R. Gentner<sup>5</sup>, Timothy R. Dallman<sup>5</sup>, Thomas W. Kirchstetter<sup>5,6</sup>, Robert A.  
7 Harley<sup>5,6</sup>, Jessica B. Gilman<sup>7,8</sup>, William C. Kuster<sup>8</sup>, Joost A. de Gouw<sup>7,8</sup>, John H. Offenberg<sup>9</sup>,  
8 Tadeusz E. Kleindienst<sup>9</sup>, Ying H. Lin<sup>10</sup>, Caitlin L. Rubitschun<sup>10</sup>, Jason D. Surratt<sup>10</sup>, and Allen H.  
9 Goldstein<sup>1,5,6</sup>

10  
11 <sup>1</sup>*Department of Environmental Science, Policy, and Management, University of California,*  
12 *Berkeley, CA, USA*

13 <sup>2</sup>*Chemical Sciences Division, Lawrence Berkeley National Laboratory, Berkeley, CA, USA*

14 <sup>3</sup>*Aerosol Dynamics Inc., Berkeley, CA, USA*

15 <sup>4</sup>*Department of Chemistry, University of California, Berkeley, CA, USA*

16 <sup>5</sup>*Department of Civil and Environmental Engineering, University of California, Berkeley, CA,*  
17 *USA*

18 <sup>6</sup>*Environment Energy Technologies Division, Lawrence Berkeley National Laboratory, Berkeley,*  
19 *CA, USA*

20 <sup>7</sup>*Cooperative Institute for Research in the Environmental Sciences (CIRES), University of*  
21 *Colorado, Boulder, CO, USA*

22 <sup>8</sup>*NOAA Chemical Sciences Division, Boulder, CO, USA*

23 <sup>9</sup>*National Exposure Laboratory, Office of Research and Development, Environmental Protection*  
24 *Agency, Research Triangle Park, NC, USA*

25 <sup>10</sup>*Department of Environmental Sciences and Engineering, Gillings School of Global Public*  
26 *Health, University of North Carolina at Chapel Hill, NC, USA*

27

28 A. W. H. Chan, D. R. Gentner, A. H. Goldstein, G. Isaacman, C. R. Ruehl, and D. R. Worton,  
29 Department of Environmental Science, Policy, and Management, 250 Hilgard Hall, University of  
30 California, Berkeley, CA 94720, USA. (arthurchan@berkeley.edu; ahg@berkeley.edu)

31 T. R. Dallmann and R. A. Harley, Department of Civil and Environmental Engineering, 760  
32 Davis Hall, University of California, Berkeley, CA 94720, USA.

33 J. A. de Gouw, J. B. Gilman and W. C. Kuster, NOAA ESRL & CIRES, 325 Broadway CSD7,  
34 Boulder, CO 80305, USA.

35 T. W. Kirchstetter, Lawrence Berkeley National Laboratory, 1 Cyclotron Road, MS 70-108B,  
36 Berkeley, CA 94720, USA.

37 T. E. Kleindienst, J. H. Offenberg, National Exposure Research Laboratory, U.S. Environmental  
38 Protection Agency, Research Triangle Park, NC 27711, USA.

39 Y. H. Lin, C. L. Rubitschun, and J. D. Surratt, Campus Box 7431, University of North Carolina  
40 at Chapel Hill, Chapel Hill, NC 27599, USA.

41 T. Nah and K. R. Wilson, Lawrence Berkeley National Laboratory, 1 Cyclotron Road, MS 6R21,  
42 Berkeley, CA 94720, USA.

43

44 **Abstract**

45 Recent studies suggest that semivolatile organic compounds (SVOCs) are important precursors  
46 to secondary organic aerosol (SOA) in urban atmospheres. However, knowledge of the chemical  
47 composition of SVOCs is limited by current analytical techniques, which are typically unable to  
48 resolve a large number of constitutional isomers. Using a combination of gas chromatography  
49 and soft photoionization mass spectrometry, we characterize the unresolved complex mixture  
50 (UCM) of aliphatic hydrocarbons observed in Pasadena, CA (~16 km NE of downtown Los  
51 Angeles) and Bakersfield, CA during CalNex 2010. Knowledge of molecular structures,  
52 including carbon number, alkyl branching, and number of rings, provides important constraints  
53 on the rate of atmospheric processing, as the relative amounts of branched and linear alkanes are  
54 shown to be a function of integrated exposure to hydroxyl radicals. Emissions of semivolatile  
55 branched alkanes from fossil-fuel related sources are up to an order of magnitude higher than  
56 those of linear alkanes, and the gas-phase OH rate constants of branched alkanes are ~30%  
57 higher than their linear isomers. Based on a box model considering gas/particle partitioning,  
58 emissions and reaction rates, semivolatile branched alkanes are expected to play a more  
59 important role than linear alkanes in photooxidation of the UCM and subsequent transformations  
60 into SOA. Detailed speciation of semivolatile compounds therefore provides essential  
61 understanding of SOA sources and formation processes in urban areas.

62

## 63 **Introduction**

64 Organic matter represents a major fraction of ambient aerosol. A large fraction of organic aerosol  
65 (OA) is formed from oxidation of gas-phase hydrocarbons, and is known as secondary organic  
66 aerosol (SOA) [Zhang *et al.*, 2007]. However, current atmospheric models typically  
67 underestimate the budget of SOA, highlighting a lack of understanding in the sources and

68 transformation processes of organic compounds in the atmosphere [*Goldstein and Galbally,*  
69 2007]. Recently, it has been proposed that oxidation of semivolatile organic compounds  
70 (SVOCs) is a major source of SOA, particularly in urban atmospheres [*Pye and Seinfeld,* 2010;  
71 *Robinson et al.,* 2007]. SVOCs are defined as compounds which have effective saturation  
72 concentrations ( $C^*$ ) between 0.1 and 10  $\mu\text{g m}^{-3}$ . Owing to the low vapor pressures of SVOCs and  
73 of their subsequent reaction products, oxidation of SVOCs is expected to have significantly  
74 higher SOA yields than more volatile precursors, and, despite lower emissions, could dominate  
75 SOA formation in urban areas. Models that incorporate transformations of SVOCs to SOA yield  
76 better predictions of the total amount of SOA and its seasonal variability [*Hodzic et al.,* 2010;  
77 *Robinson et al.,* 2007]. However, these models tend to underestimate the observed O/C ratios,  
78 and fail to capture the diurnal variations [*Hodzic et al.,* 2010] and vertical profiles of SOA  
79 [*Heald et al.,* 2011], suggesting that the atmospheric chemistry of SVOCs leading to SOA  
80 formation is poorly understood. Their relative oxidation rates and mechanisms, the two key  
81 factors that determine the amount and properties of SOA formed, are currently extrapolated from  
82 those of smaller carbon numbers.

83

84 Detailed knowledge of the identities and chemistry of semivolatile compounds is challenging, as  
85 the chemical composition is highly complex and current analytical techniques are unable to  
86 separate and identify these compounds. While gas chromatography-mass spectrometry (GC/MS)  
87 has been the most common method for speciating these compounds, atmospheric sources often  
88 emit a large number of compounds, which cannot be separated by traditional GC methods. As a  
89 result, many atmospheric samples contain a large unresolved peak in chromatographic analyses,  
90 often referred to as the unresolved complex mixture (UCM) [*Schauer et al.,* 1999]. The UCM

91 can account for more than 80% of semivolatile emissions from diesel [Schauer *et al.*, 1999] and  
92 gasoline engines [Schauer *et al.*, 2002], representing a major fraction of SVOCs in urban areas  
93 [Williams *et al.*, 2010b]. Furthermore, the UCM is ubiquitous in environmental chemistry, often  
94 found in samples associated with fossil fuel use [Frysiner *et al.*, 2003; Nelson *et al.*, 2006;  
95 Ventura *et al.*, 2008].

96  
97 The UCM is thought to contain a large number of constitutional isomers, most of which are  
98 linear (also termed straight-chained or normal), branched, or cyclic alkanes [Mao *et al.*, 2009]. In  
99 contrast, aromatic compounds comprise only a minor fraction of the UCM [Van Deursen *et al.*,  
100 2000]. Owing to the challenges in speciating alkane isomers, SVOCs have typically been  
101 classified by volatility only, inferred from thermodenuder measurements or gas chromatography  
102 retention times [Grieshop *et al.*, 2009; Presto *et al.*, 2012], which then serve as inputs into the  
103 aforementioned models [Hodzic *et al.*, 2010; Pye and Seinfeld, 2010]. Information about  
104 molecular structures is generally overlooked. However, the number of rings and alkyl branches  
105 in alkanes strongly affect their oxidation chemistry and their SOA yields [Lim and Ziemann,  
106 2009; Tkacik *et al.*, 2012]. Molecular structure also plays an important role in other degradation  
107 pathways of environmentally relevant complex mixtures [Nelson *et al.*, 2006]. As a result,  
108 knowledge of molecular structure is crucial to understanding the sources and environmental fate  
109 of these hydrocarbons.

110  
111 The main objective of this work is to characterize the molecular composition of ambient UCM,  
112 classify the components by molecular structure for use in future models of urban atmospheres,  
113 and use this detailed information to understand their atmospheric processing and SOA formation.

114 Previously, we have demonstrated that constitutional isomers present in diesel fuel can be  
115 characterized using gas-chromatography coupled to vacuum ultraviolet ionization mass  
116 spectrometry (GC/VUV-MS) [Isaacman *et al.*, 2012a]. We combine this technique with  
117 comprehensive 2-dimensional gas chromatography (GC×GC/VUV-HR-TOFMS) to characterize  
118 in detail the composition of ambient semivolatile compounds observed during the California  
119 Research at the Nexus of Air Quality and Climate Change (CalNex) campaign in summer 2010.  
120 The samples were collected at two urban sites in California (Pasadena, CA and Bakersfield, CA).  
121 Using detailed speciated measurements of linear, branched and cyclic alkanes in the UCM, we  
122 constrain their relative oxidation rates and provide valuable insights into their sources,  
123 processing and relative contributions to SOA formation. The utility of the analytical technique in  
124 resolving aliphatic, aromatic and polar species observed in the ambient atmosphere is also  
125 discussed.

126

## 127 **Methods**

### 128 *Sampling locations*

129 The samples described in this manuscript were collected at two urban sites in California  
130 (Pasadena, CA and Bakersfield, CA) as part of the CalNex field campaign in the summer of 2010  
131 ([www.esrl.noaa.gov/csd/calnex/](http://www.esrl.noaa.gov/csd/calnex/)). Pasadena sampling was conducted on the campus of the  
132 California Institute of Technology, ~16 km NE of downtown Los Angeles (hereafter referred to  
133 as the LA site). Two PM<sub>2.5</sub> samples from the LA site, collected on Sunday May 30 (3:00 – 6:00  
134 PM local time) and Saturday June 5 (midnight – 11 PM local time), were selected for analysis  
135 under VUV ionization, as these two days represented different degrees of photochemical aging,  
136 the significance of which will be discussed below. 54 samples from the intensive filter sampling

137 periods, collected at a time resolution of 3 to 6 hours, were analyzed under electron impact (EI)  
138 ionization. Sampling at the Bakersfield site was conducted at the southeast edge of the city, co-  
139 located with other instruments participating in the field campaign. Two 23-hour samples,  
140 collected on Friday June 18 and Wednesday June 23 from midnight to 11 PM local time, were  
141 selected for VUV analysis. These two samples, along with 32 other daily (midnight – 11 PM)  
142 filter samples were also analyzed under EI. All samples collected from the Pasadena site were  
143 collected on quartz fiber filters (Tissuquartz™ Filters, 2500 QAT-UP, Pall Life Sciences), which  
144 were 20 cm × 25 cm, allowing for high-volume PM<sub>2.5</sub> sampling at ~1 m<sup>3</sup> min<sup>-1</sup>. All samples  
145 collected from the Bakersfield site were collected on 86 cm<sup>2</sup> quartz fiber filters (Pall Life  
146 Sciences); however, medium-volume PM<sub>2.5</sub> sampling at 226 L min<sup>-1</sup> was conducted. All filters  
147 were pre-baked at 550 °C to remove any organic contaminants. Filter samples were stored in a  
148 freezer at -18 °C until chemical analysis. Field blanks were collected every 7–10 days by  
149 placing a pre-fired quartz fiber filter into the sampler for 15 min before removing and storing in  
150 the same manner as the field samples. Analysis of both field and laboratory blanks showed no  
151 significant aliphatic contaminants on pre-fired quartz filters.

152  
153 Additional samples collected during a study conducted at the Caldecott Tunnel in Oakland, CA  
154 were also analyzed for comparison [Dallmann *et al.*, 2012]. Here we focus our analysis on 2  
155 weekday filter samples collected in the gasoline-only bore, and 5 samples collected in the mixed  
156 gasoline/diesel bore (4 weekday and 1 weekend samples). Emissions during collection of the 2  
157 weekday samples from the gasoline-only bore and the weekend sample from the mixed bore are  
158 expected to be dominated by gasoline vehicles (3 “gasoline-dominated” samples), while  
159 emissions during the 4 weekday samples in the mixed bore are expected to be dominated by

160 diesel vehicles (4 “diesel-dominated” samples). In addition to thermal desorption of filter  
161 samples, SAE 10W-30 motor oil and 3 samples of crude oil extracted and refined in the San  
162 Joaquin Valley region were also analyzed for their chemical composition. The origins of the  
163 crude oil samples are confidential for proprietary reasons.

164

#### 165 *Speciation of semivolatile hydrocarbons*

166 Selected samples were analyzed using comprehensive 2-dimensional gas chromatography  
167 coupled to a vacuum-ultraviolet high-resolution time-of-flight mass spectrometer  
168 (GC×GC/VUV-HRTOFMS). Filter punches (total area of 1.6 cm<sup>2</sup>) were thermally desorbed at  
169 320 °C under helium using a thermal desorption system and autosampler (TDS3 & TDSA2,  
170 Gerstel). Desorbed samples were focused at 20 °C on a quartz wool liner in a cooled injection  
171 system (CIS4, Gerstel) before they were introduced into a gas chromatograph (GC, Agilent  
172 7890). For motor oil and crude oil, samples diluted in chloroform were directly injected via a  
173 septumless inlet into the GC.

174

175 Comprehensive GC×GC was performed using a 60 m × 0.25 mm × 0.25 μm non-polar capillary  
176 column (Rxi-5Sil MS, Restek) for the first-dimension separation (by volatility), and a medium-  
177 polarity second dimension column (1 m × 0.25 mm × 0.25 μm, Rtx-200MS, Restek). A dual-  
178 stage thermal modulator (Zoex), consisting of a guard column (1 m × 0.25 mm, Rxi, Restek),  
179 was used as the interface between the two columns, where the effluent from the first column was  
180 cryogenically focused and periodically heated for rapid transfer into the second column. The  
181 modulation period was 2.4 seconds.

182

183 Effluent from the second column was analyzed using a high-resolution ( $m/\Delta m \sim 4000$ ) time-of-  
184 flight mass spectrometer (HTOF, Tofwerk) coupled to the Advanced Light Source at Lawrence  
185 Berkeley National Laboratory. Single photon ionization by the vacuum ultraviolet (VUV) beam  
186 used here is similar to that reported previously [Isaacman *et al.*, 2012a]. In brief, photons of 10.5  
187 eV with an energy distribution width of 0.2 eV and an intensity of  $\sim 10^{15}$  photons  $s^{-1}$  were  
188 generated by the Chemical Dynamics Beamline (9.0.2). The photon beam was introduced  
189 orthogonally to the GC effluent, and ionized molecules were accelerated into the extraction  
190 region. Since the ionization energies of most organic compounds are between 8 and 11 eV, the  
191 minimal excess energy (compared to electron impact ionization at 70 eV) limits fragmentation of  
192 ionized molecules, allowing for significant detection of the molecular ions ( $M^{++}$ ). The ion  
193 chamber was maintained at 150 °C to minimize fragmentation. All LA and Bakersfield samples  
194 were also analyzed under EI at 70 eV, using a standard tungsten filament.

195  
196 The molecular ion signals for linear, branched and cyclic alkanes under VUV ionization are used  
197 as the basis for quantification [Isaacman *et al.*, 2012b]. Details about the calibration method  
198 based on molecular structures are described in Appendix A of the Supplementary Material. The  
199 adjusted molecular ion signals were then quantified based on known quantities (5 ng each) of  
200 perdeuterated internal standards (*n*-hexadecane- $d_{34}$ , *n*-eicosane- $d_{42}$ , *n*-tetracosane- $d_{50}$ , and *n*-  
201 octacosane- $d_{58}$ , C/D/N Isotopes) spiked onto the filter punches prior to analysis. In quantifying  
202 the aliphatic hydrocarbons, only the UCM region of the chromatogram was considered (second  
203 dimension retention time between 0.4 and 0.9 seconds). Polycyclic aromatic hydrocarbons  
204 (PAHs) and highly oxygenated compounds are not expected to elute in this region. In addition,  
205 signals of oxygen-containing molecular ions were removed by high-mass-resolution data

206 processing procedures [Isaacman *et al.*, 2012b], such that only aliphatic molecular ions ( $C_xH_y^+$ )  
207 were considered for quantification. All data processing and visualization of GC×MS data were  
208 performed using custom code written in Igor 6.2.2 (Wavemetrics), while visualization of 2-  
209 dimensional chromatography data and detection of chromatographic peaks were carried out  
210 using GC Image software (LLC).

211

### 212 *Other measurements*

213 Co-located measurements of volatile organic compounds (VOCs) by *in situ* GC/MS are also used  
214 for comparison. Details of the GC/MS technique used in LA are described by *Gilman et al.*  
215 [2010]. Average photochemical age of air masses at the LA site was calculated using the ratio of  
216 1,2,4-trimethylbenzene to benzene [Borbon *et al.*, 2012; Parrish *et al.*, 2007]. GC/MS  
217 measurements of light hydrocarbons at the Bakersfield site were used for source identification  
218 purposes. Details of the GC/MS technique are described by *Gentner et al.* [2012].

219

## 220 **Results and Discussion**

### 221 *Resolving the UCM using GC×GC and GC×MS*

222 Figure 1 shows the total integrated ion chromatogram of the LA and Bakersfield samples under  
223 VUV ionization. Similar to previous work using GC×GC to analyze atmospheric samples, PAHs  
224 and oxygenated compounds, such as acids and ketones, are readily separated from aliphatic  
225 compounds [Worton *et al.*, 2012]. Examples of these peaks are provided in Fig. S-2 in the  
226 Supplementary Material. Despite the increased peak capacity, there is still a large unresolved  
227 “hump” in the nonpolar region of the chromatogram, representing the UCM. The dominance of  
228 the UCM is present in most ambient samples that were analyzed by EI. The inability of GC×GC

229 to resolve these aliphatic hydrocarbons is likely due to the large number of possible  
230 constitutional isomers [Goldstein and Galbally, 2007], resulting in overlapping volatilities. In  
231 addition, even though the isomers are structurally different, all hydrocarbons are nonpolar and  
232 are essentially unretained in a polar column, resulting in poor second-dimension resolution.  
233 Further chromatographic separation of the UCM can be performed using other column pairings  
234 [Nelson *et al.*, 2006], reversed-phase chromatography [Vogt *et al.*, 2007], or coupled liquid  
235 chromatography-GC×GC [Mao *et al.*, 2009]. However, in analyzing atmospheric samples, a  
236 polar column is preferred owing to the need for also separating aromatic and oxygenated  
237 compounds which are prevalent. Orthogonal separation by volatility and polarity also allows for  
238 convenient inputs into 2-dimensional frameworks used to model evolution of organic compounds  
239 in the atmosphere [Isaacman *et al.*, 2011; Jimenez *et al.*, 2009].

240  
241 In this work, the aliphatic UCM is characterized by a novel method using a combination of gas  
242 chromatography and soft VUV photoionization. Traditional GC/MS employs electron impact at  
243 70 eV as the ionization technique, which imparts a large amount of excess energy and causes  
244 extensive fragmentation. While the fragmentation mass spectra can in many cases be useful for  
245 compound identification, aliphatic compounds have almost identical fragmentation patterns, with  
246 a large fraction of signal at  $m/z$  41, 43, 55, 57, 69, 71 etc. (corresponding to  $C_xH_{2x+1}^+$  and  $C_xH_{2x-1}^+$   
247 ions, where  $x$  is typically between 3 and 6). As a result, these compounds cannot be distinguished  
248 from each other, as illustrated in Fig. 2a. Soft ionization retains the identity of a molecule by  
249 maximizing the relative signal of the molecular ion, albeit at the loss of ionization efficiency.  
250 Similar to aliphatic compounds in diesel fuel shown in our previous study, coupling soft  
251 ionization with volatility-based GC separation allows hydrocarbons in the UCM in the ambient

252 atmosphere to fall into distinguishable patterns in a GC×MS plot (Fig. 2b) [Isaacman *et al.*,  
253 2012a; Wang *et al.*, 2005].

254  
255 In the GC×MS diagram, each cluster corresponds to a carbon number. Within each carbon  
256 number, the molecular formulas can be identified from molecular weights of parent ions, shown  
257 on the y-axis. As a result, the complex mixture can be speciated by number of carbon atoms and  
258 the number of double bond equivalents,  $N_{DBE}$ , which is the total number of rings and C=C double  
259 bonds. In the samples from both urban sites, the observed UCM lies in the range of 20 to 25  
260 carbon atoms. In this range, alkanes have saturation vapor pressures between  $9 \times 10^{-8}$  and  $9 \times 10^{-6}$   
261 torr (saturation concentrations between approximately  $2 \mu\text{g m}^{-3}$  and  $200 \mu\text{g m}^{-3}$  at 298K), and  
262 are therefore semivolatile and expected to exist in both the particulate and gas phases under  
263 atmospheric loadings [Williams *et al.*, 2010a]. It must be noted that smaller, more volatile  
264 hydrocarbons are expected to be abundant, but cannot be effectively and quantitatively collected  
265 on quartz filter samples used in this study. Most hydrocarbons observed have  $N_{DBE} < 6$ . Alkenes  
266 in this molecular weight range are highly reactive and are not expected to be significant in  
267 atmospheric samples. While alkene production from thermal decomposition of labile compounds  
268 (containing oxygen or nitrogen) cannot be ruled out, the distributions across different  $N_{DBE}$   
269 classes were similar to those observed in unoxidized motor oil [Isaacman *et al.*, 2012b].  
270 Therefore, cyclic alkanes (not alkenes) are expected to dominate aliphatic compounds observed  
271 with  $N_{DBE} > 0$  in Bakersfield and LA, similar to alkanes found in motor oil.

272  
273 Within each DBE class, gas chromatography provides separation of isobaric compounds (with  
274 the same molecular formula) by volatility. Since branched alkanes are more volatile than their

275 linear counterparts of the same carbon number, they elute earlier relative to the respective linear  
276 alkane from the first dimension column. As shown in Fig. 2c, good chromatographic resolution  
277 is achieved for linear and branched alkanes with  $N_{DBE} = 0$ . Unlike in diesel fuel [Isaacman *et al.*,  
278 2012a] but as observed in motor oil [Isaacman *et al.*, 2012b], structural isomers are not well  
279 resolved for  $N_{DBE} > 0$ . This is most likely due to the higher carbon number range of the ambient  
280 UCM, and, hence, a greater number of possible *E/Z* configurations. As a result, mass  
281 concentrations of branched isomers are only reported for acyclic alkanes ( $N_{DBE} = 0$ ). Following  
282 the naming convention of our previous work, we refer to branched isomers which contain *x* alkyl  
283 branches as B*x* isomers. For example, B0 refers to the linear alkane, B1 refers to alkanes with 1  
284 alkyl branch etc.

285  
286 To the authors' knowledge, this work represents the most detailed characterization of the UCM  
287 in atmospheric samples to date. The calibrated masses of linear, branched and cyclic alkanes for  
288 carbon numbers between 20 and 25 are shown in Fig. 3. The relative ratios of total branched  
289 alkanes to linear alkanes (hereafter referred to as B/N ratio) vary greatly between the two urban  
290 sites, from ~1 in the June 5 LA sample to >10 in both Bakersfield samples, shown in Fig. 4.

291  
292 *Processing of semivolatile hydrocarbons in Los Angeles, CA*

293 In both LA samples analyzed under VUV photoionization, while the unresolved "hump" is  
294 visible in the chromatogram, aromatic and more polar compounds have a higher total integrated  
295 ion signals than the UCM (Fig. 1a). The most abundant isomer for each carbon number is the  
296 linear alkane, accounting for >30% of the total acyclic alkane mass. The two samples analyzed  
297 under VUV represent two different periods in the field campaign. From June 2 through June 6,

298 there was a steady build-up of pollutants due to periodic entrainment of the residual layer aloft,  
299 causing fresh emissions in the boundary layer to be mixed with aged pollutants that remained in  
300 the basin [Pollack *et al.*, 2012]. On May 30, no such build-up was observed. Owing to this  
301 difference in meteorological conditions, the integrated OH exposure, calculated from the ratios  
302 of 1,2,4-trimethylbenzene (1,2,4-TMB) to benzene [Borbon *et al.*, 2012], was higher during  
303 collection of the June 5 sample ( $4.8 \times 10^{10}$  molec cm<sup>-3</sup> s) than that of the May 30 sample ( $2.6 \times$   
304  $10^{10}$  molec cm<sup>-3</sup> s).

305  
306 The B/N ratios of C<sub>21</sub>–C<sub>24</sub> hydrocarbons in the May 30 sample are higher than those in the June 5  
307 sample, suggesting that branched alkane isomers are consumed more rapidly relative to the linear  
308 isomers of the same carbon number. Since the aliphatic hydrocarbons in the UCM are  
309 predominantly saturated, their primary sink in the atmosphere is reaction with OH radicals.  
310 Although compounds in this volatility range exist in both the gas and particle phases, C<sub>21</sub>–C<sub>24</sub>  
311 hydrocarbons are sufficiently volatile that their gas phase reactions with OH are dominant over  
312 particle-phase reactions at ambient levels of OA concentrations [Lambe *et al.*, 2009]. We  
313 therefore expect that the change in B/N ratios is primarily a result of differences in gas-phase  
314 reaction rates with OH radicals, and the decay can be described by the following equation:

$$315 \quad \left(\frac{B}{N}\right)_{sample} = \left(\frac{B}{N}\right)_0 e^{(k_N f_N - k_B f_B) \int [OH] dt} \quad (1)$$

316 where (B/N)<sub>0</sub> is the B/N ratio at the source; (B/N)<sub>sample</sub> is the B/N ratio of each individual  
317 sample;  $k_B$  is the average OH reaction rate of all branched isomers (cm<sup>3</sup> molec<sup>-1</sup> s<sup>-1</sup>), which is  
318 treated here as an unknown;  $k_N$  is the OH reaction rate of the linear alkane (cm<sup>3</sup> molec<sup>-1</sup> s<sup>-1</sup>),  
319 calculated from structural-reactivity relationships [Kwok and Atkinson, 1995];  $f_N$  is the average  
320 gas-phase fraction of the linear isomer;  $f_B$  is the average gas-phase fraction of branched isomers,

321 and  $\int [OH]dt$  is the integrated OH exposure ( $\text{molec cm}^{-3} \text{ s}$ ) for that sample, calculated from the  
322 1,2,4-TMB to benzene ratios [Borbon *et al.*, 2012]. Equation (1) is similar in form to previous  
323 investigation of hydrocarbons clocks for gas-phase oxidation, with one notable exception. Here  
324 we include the effect of gas-particle partitioning, which reduces the fractions of alkane species in  
325 the gas phase available for OH reactions. The gas-phase fraction for each filter data point is  
326 calculated individually based on known vapor pressures [Pankow and Asher, 2008; Williams *et*  
327 *al.*, 2010a], total OA mass concentrations measured by the Aerodyne Aerosol Mass Spectrometer  
328 (AMS) and temperature. Both OA mass concentrations and temperatures were similar between  
329 the two filter sampling periods (at  $7 \mu\text{g m}^{-3}$  and 290K). For the data shown in Fig. 5, we assume  
330 that  $f_N$  and  $f_B$  are constant in order to derive  $k_B$  for each carbon number.

331  
332 To investigate the relationship between B/N ratios and OH exposure, the B/N ratios at the source  
333 (corresponding to zero OH exposure) must be known. Since the major contributor of  
334 hydrocarbons in the LA Basin is likely motor vehicles [Williams *et al.*, 2010b], the B/N ratios of  
335 hydrocarbons in the LA ambient samples are compared to those in fresh vehicular exhaust,  
336 measured during a tunnel study in Oakland, California. Here we focus on the branched and linear  
337 acyclic alkanes between  $C_{21}$  and  $C_{24}$ . The average B/N ratios of these alkanes in all 7 tunnel  
338 samples are presented in Fig. 4. There were no systematic differences in B/N ratios between  
339 diesel-dominated and gasoline-dominated samples in this carbon number range, so here we  
340 report the standard deviation in the 7 samples to be the uncertainty in B/N ratios for each carbon  
341 number. The average B/N ratios observed in these tunnel samples, which are higher than those  
342 observed in the LA samples, serve as additional data points corresponding to zero OH exposure  
343 at the source. Assuming that the decrease in B/N ratio is entirely due to photooxidation, the

344 relative reaction rates of the branched isomers can be estimated from the decay of B/N ratios. A  
345 plot of B/N ratio versus OH exposure is shown in Fig. 5. From regression using equation (2), a  
346 value for  $k_B$  for each carbon number can be derived from the slope of the best-fit line ( $f_N k_N -$   
347  $f_B k_B$ ). In general, the average rate constants of branched alkane isomers are 21–35 % higher than  
348 that of the linear alkanes (see Table 1).

349  
350 The uncertainties in the regressions on the B/N ratios measured using VUV are considerable,  
351 owing to the limited number of samples analyzed using this technique. To further constrain the  
352 dependence of B/N ratios on photochemical processing, analysis of samples covering a wide  
353 range of photochemical processing is needed. As mentioned before, under electron impact,  
354 detailed speciation, similar to that achieved in Fig. 3, is difficult owing to extensive  
355 fragmentation and co-elution of isomers. However, some B0 (linear) and B1 isomer peaks can be  
356 resolved from other isomers, and their retention times and molecular formulas are confirmed by  
357 VUV analysis, as shown in Fig. 6. Each linear isomer coelutes with a B2 isomer with one more  
358 carbon atom, but, based on observations from VUV, this B2 isomer is expected to contribute  
359 <15% of the total ion signal for C<sub>22</sub>–C<sub>24</sub> alkanes in the LA samples. Other isomers, such as B2  
360 isomers and isomers with  $N_{DBE} > 0$  remain unresolved under EI. The ratio of B1 to linear isomers  
361 (B1/N ratios) for each carbon number was calculated from the background-subtracted signals on  
362 C<sub>4</sub>H<sub>9</sub><sup>+</sup> ( $m/z$  57), the most common alkane fragment ion. Using this method, more reliable  
363 estimates of  $k_B$  are derived from EI data, which consist of a larger number of samples. However,  
364 temperature and OA mass can no longer be assumed to be constant, and these factors critically  
365 determine gas-phase fractions and hence oxidation rates of SVOCs. For the EI data set, we first  
366 determine the average photochemical age for each sample, assuming an [OH] of  $2 \times 10^6$  molec

367  $\text{cm}^{-3}$ . An average temperature and OA mass, to which each air plume represented by the sample  
368 has been exposed, are then determined. With this information, a B1/N ratio for each sample can  
369 be calculated for any given  $k_{B1}$  and  $(B1/N)_0$  using Equation (1), and optimal values for these two  
370 parameters are determined that minimizes the absolute error between calculated and observed  
371 B/N ratios derived from EI data. The regressions are shown in Fig S-3 in the Supplementary  
372 Material. Values for  $k_{B1}$  are consistent with those derived from VUV data, as shown in Table 1,  
373 confirming that B1 isomers of  $C_{22}$ – $C_{24}$  alkanes are consumed more rapidly than linear isomers.  
374 Figures 7a–7c show the diurnal profiles of the B1/N ratios, and the minima in B1/N ratios occur  
375 between late morning and early afternoon. The daytime minima are likely a result of higher OH  
376 concentrations and greater extent of oxidation. In a later section, we will rule out higher daytime  
377 temperatures (which alters gas/particle partitioning) to be the cause of the observed drop in B1/N  
378 ratios.

379  
380 Structure-reactivity predictions for linear and branched alkanes with 21 to 24 carbons are  
381 summarized in Table 1. The predicted rate constants of branched alkanes are 1–8% higher than  
382 those of the linear isomers, lower than the ratios observed. Under these predictions, a  
383 combination of a tertiary and a primary carbon atom have higher OH reaction rates than two  
384 secondary carbon atoms if the tertiary carbon atom is not at the 2-position [*Kwok and Atkinson,*  
385 1995]. While small ( $<C_5$ ) branched hydrocarbons have lower OH rate constants than their linear  
386 isomers, it is more statistically likely for  $C_{21}$ – $C_{24}$  alkanes that alkyl branching will instead occur  
387 at the 3- or higher positions, resulting in higher predicted OH rate constants. It is also noteworthy  
388 that preferred depletion of branched isomers was also observed during experimental studies of  
389 heterogeneous oxidation of motor oil particles [*Isaacman et al., 2012b*]. In those experiments,

390 oxidation is expected to occur in the particle phase owing to the high particulate loadings, and  
391 the ratios of the rate constants ( $k_B/k_N = 1.28$ ) reported are roughly consistent with those of gas-  
392 phase rate constants observed in this work.

393  
394 While the possibility of additional sources with low B/N ratios cannot be ignored, differences in  
395 this ratio caused by some potential primary sources of aliphatic hydrocarbons can be ruled out.  
396 There is no odd carbon preference in this range of carbon numbers, indicating that plant wax is  
397 not a major contributor to aliphatic compounds in the UCM. Also, wood burning markers, such  
398 as dehydroabietic acid and retene, were not observed at significant concentrations, indicating that  
399 the trend in B/N ratios is not caused by emissions of linear alkanes from biomass or biofuel  
400 burning. No additional source of linear alkanes contributing to the lower B/N ratios in more aged  
401 samples has yet been identified. We also considered whether the changes in B/N ratio could be  
402 caused by a difference in fleet between Oakland, CA and the LA Basin, but concluded that  
403 differences would likely be minimal across the state. Additionally, this would only affect B/N  
404 ratios of the emission source  $(B/N)_0$ , and would be unlikely to cause B/N ratios to decrease with  
405 photochemical age as demonstrated.

406

#### 407 *Source of semivolatile hydrocarbons in Bakersfield, CA*

408 Semivolatile and non-volatile hydrocarbons in Bakersfield appear to originate from a broader  
409 combination of sources than in LA. First, the high concentrations of odd-number *n*-alkanes ( $C_{23}$   
410 and  $C_{25}$ , see Fig. 3d) suggest that plant wax could be a major source. The carbon number  
411 preference index (CPI) of *n*-alkanes between  $C_{21}$  and  $C_{33}$  is given by the following equation  
412 [Marzi *et al.*, 1993]:

413 
$$CPI = \frac{\sum_{i=10}^{15} C_{2i+1} + \sum_{i=11}^{16} C_{2i+1}}{2 \sum_{i=10}^{15} C_{2i}} \quad (2)$$

414 where  $C_x$  is the concentration of  $n$ -alkanes with  $x$  carbon atoms. The CPI of Bakersfield samples  
415 were consistently above 2, indicating a strong contribution of plant wax. In contrast, the average  
416 CPI of LA samples were below 1.4. This is consistent with factor analysis using AMS and FTIR  
417 data from CalNex Bakersfield, which suggests that up to 10% of organic aerosol is likely  
418 vegetative detritus [Liu *et al.*, 2012].

419  
420 Using GC/VUV, the alkane isomers in the UCM are classified into branched, cyclic and linear  
421 alkanes based on molecular weights and GC retention times. Branched isomers dominate over  
422 linear isomers in Bakersfield, with B/N ratios greater than 10. These B/N ratios are inconsistent  
423 with those measured in the LA samples, and are even higher than those observed in fresh motor  
424 vehicle exhaust from the tunnel samples. Since semivolatile branched alkanes react with OH  
425 radicals faster than linear isomers both theoretically (from structure-reactivity relationships) and  
426 in flow tube experiments [Isaacman *et al.*, 2012b], photochemical processing is not expected to  
427 increase the B/N ratios from those of motor vehicle UCM to those observed in Bakersfield.

428 While factor analysis of particle-phase molecular markers suggest that a major source of linear  
429 alkanes is motor vehicles [Zhao *et al.*, 2012], the high B/N ratio of the UCM suggests that there  
430 is a also large source of predominantly branched semivolatile hydrocarbons in addition to motor  
431 vehicles contributing significantly to the Bakersfield UCM.

432  
433 To investigate the temporal trends in this potentially large source of semivolatile branched  
434 hydrocarbons, the B1/N ratios are derived from EI data using the method previously described.  
435 B1/N ratios of only  $C_{23}$  and  $C_{24}$  can be reliably determined from EI data, owing to co-elution of

436 other linear alkanes with B2 isomers (see Fig. 6). Extensive comparisons to speciated VOC  
437 concentrations in the region showed poor correlations of B1/N ratios to volatile tracers of known  
438 sources, such as gasoline and diesel vehicles, and natural gas production. One potential source of  
439 semivolatile hydrocarbons is the oil extraction and refining operations in the area, as Bakersfield  
440 is surrounded by numerous oil and gas fields, and two refineries are within 15 km of the  
441 sampling site. The isomer distributions of C<sub>21</sub>–C<sub>24</sub> hydrocarbons of the ambient Bakersfield  
442 samples are therefore compared to those of 3 crude oil samples and one motor oil (SAE 10W-30)  
443 sample. As shown in Fig. 8, the B/N ratios of the 3 crude oil samples vary by an order of  
444 magnitude. It is well known that the chemical composition of crude oil is highly variable, and the  
445 purpose of refining operations is to modify the chemical composition (relative concentrations of  
446 alkanes, alkenes, cycloalkanes, aromatics etc.) for fuel, oil, chemical feedstock or other uses.  
447 Lubricating oil, for example, has higher concentrations of cycloalkanes (also known as  
448 naphthenes) and branched alkanes than *n*-alkanes, as the viscosities of *n*-alkanes have stronger  
449 temperature dependence and increase significantly when motor engines heat up [Gary *et al.*,  
450 2007]. While detailed characterization of the crude oil samples is beyond the scope of this work,  
451 the highly branched alkane content observed in Bakersfield is consistent with that in motor oil  
452 and one of the 3 crude oil samples analyzed. At this point, only qualitative comparisons are  
453 possible, but based on available data the high concentrations of branched alkanes in the UCM are  
454 likely related to oil extraction and/or refining operations. In the future, detailed speciation of  
455 alkane isomers in direct emissions from oil operations could be useful in quantitatively  
456 determining their importance as a source of semivolatile hydrocarbons in this area.

457

458 *Modeling relative SOA formation from branched and linear alkanes*

459 Oxidation of semivolatile alkanes has been proposed to contribute significantly to urban SOA  
460 formation. While branched isomers tend to fragment upon oxidation, their emissions are higher  
461 and are oxidized more rapidly, because of their higher volatility and greater reactivity toward OH  
462 radicals. Using the relative loss rates from CalNex LA, we formulate a simple box model to  
463 investigate the relative contributions to SOA formation from branched and linear alkanes. Based  
464 on equation (1), the ratio of SOA mass formed from branched alkanes to that from their linear  
465 isomer for a particular carbon number can be described by:

$$466 \quad \frac{SOA_B}{SOA_N} = \left(\frac{B}{N}\right)_0 \left(\frac{1-e^{-k_B f_B \int [OH] dt}}{1-e^{-k_N f_N \int [OH] dt}}\right) \left(\frac{Y_B}{Y_N}\right) \quad (3)$$

467 where  $Y_B$  and  $Y_N$  are the SOA mass yields for a branched alkane and a linear alkane, respectively.  
468 To the authors' knowledge, there are no existing experimental measurements of SOA yields from  
469 alkanes greater than 21 carbons. Here we calculate the theoretical SOA yields using a near-  
470 explicit gas-phase oxidation mechanism and theoretical partitioning based on work by *Jordan et*  
471 *al.* [2008]. We note that the SOA yields of  $C_{21}$ – $C_{24}$  *n*-alkanes calculated from this approach are  
472 lower than those derived from extrapolating the volatility basis set parameters recommended by  
473 *Presto et al.* [2010] to this carbon number range. However, the approach by *Jordan et al.* [2008]  
474 is preferred here because the inclusion of a fragmentation mechanism is straightforward and the  
475 volatility basis set does not distinguish between different alkane isomers.

476  
477 The partitioning of alkanes between gas and aerosol phase ( $f_B$  and  $f_N$ ) depend critically on  
478 organic loading and temperature. For our base case simulation, we assume an organic loading of  
479  $10 \mu\text{g m}^{-3}$  and an average temperature of 293K, which is typical of ambient conditions during  
480 CalNex LA. For modeling the SOA yields  $Y_B$  and  $Y_N$ , we use a branching ratio of 0.30 for the  
481 fragmentation pathway in branched alkanes system, and assume it leads to a ketone with a

482 carbon number half that of the parent alkane. For linear alkanes, this branching ratio is set to 0.  
483 We assume that  $[\text{OH}]$  is constant at  $2 \times 10^6 \text{ molec cm}^{-3}$  and perform the simulation for 8 hours,  
484 the maximum photochemical age observed in LA. Figure 9 shows the ratio of SOA mass from  
485 branched alkanes to that of linear alkanes (hereafter referred to as the BNSOA ratio) for this base  
486 case scenario. The more reactive branched alkanes form SOA earlier than linear alkanes, causing  
487 the BNSOA ratio to decrease over time. However, as shown in the contour plots in Fig. 10 and in  
488 Eqn (3), the BNSOA ratio is linear with respect to  $(\text{B}/\text{N})_0$  and is therefore a stronger function of  
489 the emission ratios than photochemical age under typical urban conditions. Also, as  
490 demonstrated in previous sections, the  $(\text{B}/\text{N})_0$  can vary by an order of magnitude depending on  
491 the source. In the range of  $(\text{B}/\text{N})_0$  observed in this work, BNSOA ratio is expected to be at least  
492 0.5 for all carbon numbers, and can be greater than 10 in many cases. These results are  
493 qualitatively consistent with those from recent laboratory experiments and demonstrate these  
494 previously unresolved alkanes are dominant SOA precursors [Tkacik *et al.*, 2012].

495  
496 Figure 11 shows the relative importance of different parameters that affect the BNSOA ratio,  
497 including gas/particle partitioning ( $f_B$  and  $f_N$ ), gas-phase kinetics ( $k_B$  and  $k_N$ ), SOA yields and  
498 emission ratios. Branched alkanes have lower SOA yields owing to greater extent of  
499 fragmentation. However, as a result of their higher volatilities, larger OH rate constants and  
500 higher emissions, SOA formation from branched alkanes are expected to be up to 9 times that  
501 from linear alkanes in this carbon number range. In particular, the partitioning between gas and  
502 particle phases of the alkane precursors plays an important role in determining their availability  
503 for gas-phase OH reaction, especially for  $\text{C}_{24}$ , where the difference in gas phase fractions  
504 between linear and branched isomers are the greatest. It is therefore expected that temperature

505 and organic loading have important effects on the relative oxidation rates through gas/particle  
506 partitioning and SOA formation.

507

508 To examine these effects, we carry out sensitivity analyses by performing the simulations at  
509 different temperatures and organic mass concentrations representing the typical range of  
510 conditions during CalNex. It is important to note that the effect of temperature and organic  
511 loading on oxidation rates is opposite to that on SOA yields. Assuming gas/particle equilibrium,  
512 increasing organic mass leads to a smaller gas-phase fraction of both the alkane precursors and  
513 their oxidation products, leading to lower effective oxidation rates and higher SOA yields  
514 simultaneously. As shown in Fig. 12a, the organic loading increases the relative contribution of  
515 branched SOA, indicating that these two effects are greater for branched alkanes than for linear  
516 alkanes. Figure 12b shows the effect of temperature on BNSOA ratio. While increasing  
517 temperature increases fractions of both branched and linear alkanes in the gas phase ( $f_B$  and  $f_N$ ,  
518 respectively), it increases  $f_N$  by a larger fraction than  $f_B$ , since branched alkanes are more volatile.  
519 Owing to this shift in partitioning at higher temperatures, the relative decay of branched to linear  
520 alkanes is expected to be smaller, so the relative contribution of branched isomers to SOA is  
521 reduced. This also rules out temperature fluctuations to be the cause of the observed daytime  
522 decrease in B/N ratios of the precursor alkanes shown in Fig. 7, as higher daytime temperatures  
523 should lead to *higher* B/N ratios (of the precursor alkanes) and *lower* BNSOA ratios. Here we  
524 examine the effect of temperature on partitioning of the alkanes only, since the partitioning  
525 parameters of their oxidation products (e.g. vapor pressures, heat of vaporization) and  
526 temperature dependence of SOA yields are poorly understood.

527

528 Lastly, we used this box model to examine the effect of oxidation parameters on relative SOA  
529 formation. As expected, an increase in oxidation rate constant of branched alkane relative to that  
530 of linear alkane translates into a linear increase in BNSOA. It should be noted that the  
531 photochemical age simulated here is typical of urban conditions (3 hours). On these timescales,  
532 the effects of relative kinetics are expected to be more dominant than on longer timescales. The  
533 relative amount of fragmentation versus functionalization also determines the ratio of SOA  
534 yields, with fragmentation expected to be more significant for branched alkanes [*Lim and*  
535 *Ziemann, 2009*]. Here we show that the relative SOA formation vary linearly with changes in the  
536 branching ratio for the fragmentation pathway. These results imply that the uncertainties in  
537 estimating  $k_B$  and  $k_N$  (~20% difference between SRR predictions and ambient measurements)  
538 have small impacts on relative SOA contributions. On the other hand, more accurate estimates of  
539 branching between fragmentation and functionalization are needed to constrain SOA formation  
540 potentials from different alkane isomers.

541

## 542 **Atmospheric Implications**

543 In this work, we present detailed characterization of SVOCs observed at two different urban sites  
544 to understand the sources and processing of semivolatile alkanes. In both LA and Bakersfield  
545 samples, GC×GC analysis provides excellent separation of polar and aromatic compounds. For  
546 the aliphatic UCM, GC coupled with soft photoionization mass spectrometry, such as VUV,  
547 provides detailed characterization of alkane isomers. The unresolved complex mixture of alkane  
548 isomers was resolved by carbon number, number of rings, and, for saturated alkanes, the degree  
549 of branching. This unprecedented level of detail provides interesting insights into the  
550 photochemical processing of semivolatile hydrocarbons, which are important precursors to SOA

551 in the atmosphere. The ratio of branched to linear isomers for alkanes of the same carbon number  
552 decreased with photochemical processing in the LA Basin, consistent with a higher reaction rate  
553 of branched alkanes with OH radicals relative to linear alkanes. Detailed characterization of the  
554 UCM also provides information about sources, such as the odd carbon number preference and  
555 high relative concentrations of branched alkanes in the Bakersfield UCM consistent with the  
556 influences of plant wax and oil operations. Combining our speciated measurements (rate  
557 constants and emission ratios) and theoretical modeling (partitioning and SOA yields), branched  
558 alkanes are expected to contribute up to an order magnitude more to SOA formation than linear  
559 alkanes, despite lower SOA yields. The relative contributions depend strongly on their emission  
560 ratios and gas/particle partitioning for this range of volatility.

561  
562 These novel measurements provide a basis to understand atmospheric processing of different  
563 hydrocarbons in the UCM, especially those from fossil fuel related sources. The ability to  
564 speciate aliphatic compounds provides important constraints on both their effective oxidation  
565 rates, and potentials to form SOA. As shown in this work, branched alkanes have higher OH  
566 reaction rates and their emissions from fossil fuel related sources can be up to an order of  
567 magnitude higher than those of linear alkanes. Since branched alkanes react more rapidly with  
568 OH radicals than linear alkanes, the ratio of their concentrations serves as an indicator for degree  
569 of processing of SVOCs. This concept is similar to using VOC ratios to estimate the gas-phase  
570 photochemical age, but is more relevant to understanding SOA formation, since oxidation of  
571 SVOCs more readily forms low-volatility material. Our simple box model demonstrates that the  
572 oxidation rates of SVOC depend strongly on the fraction in the gas phase available for OH  
573 reaction. As a result, parameters which affect partitioning, such as organic loading and

574 temperature, also influence the oxidation kinetics. Quantitative measurements of gas/particle  
575 partitioning are therefore crucial to understanding the oxidation of SVOCs, which is expected to  
576 be their dominant loss process in the atmosphere. Also, when using SVOCs as source tracers or  
577 to estimate photochemical age, their gas/particle partitioning must be taken into account to  
578 accurately determine the extent of their atmospheric processing.

579  
580 Owing to differences in gas-phase oxidation chemistry, SOA yields depend strongly on  
581 molecular structure. Branched alkanes have a higher tendency to fragment upon oxidation,  
582 leading to more volatile products and lower SOA formation [*Lim and Ziemann, 2009*]. However,  
583 as demonstrated by our box model, oxidation of branched alkanes is expected to play a more  
584 important role in SOA formation as a result of higher emissions, faster gas-phase oxidation rate  
585 constants and higher volatility. In this work we focus our analysis on saturated alkanes. Cyclic  
586 alkanes retain the carbon backbone after ring cleavage, resulting in higher SOA yields than linear  
587 alkanes. Also, their observed emissions are greater than those of saturated alkanes. Their  
588 contributions to urban SOA formation are therefore potentially important, and accurate modeling  
589 will require a combination of speciated measurements using GC/VUV and laboratory studies into  
590 their oxidation chemistry and SOA formation mechanisms [*Lim and Ziemann, 2009; Tkacik et*  
591 *al., 2012*].

592  
593 Since SOA yields depend strongly on molecular structure, classification of organic species by  
594 volatility alone fails to fully capture SOA formation potential. Speciation by carbon number,  
595 number of rings and alkyl branching shown in this work provides detailed knowledge of both  
596 volatility and molecular structure, and hence insights into SOA formation from the UCM, the

597 major component in many SVOC sources. More detailed chemical characterization of SVOCs  
598 may also give crucial information about their sources. With more time-resolved samples,  
599 measurements of compounds speciated by molecular structure can be more broadly applied in  
600 factor analysis and can serve as valuable inputs for source attribution. Ultimately, despite the  
601 complexity of organic mixtures, detailed speciation is an important direction providing essential  
602 understanding of emission sources and their environmental fates.

603

#### 604 **Acknowledgements**

605 This research was supported by the National Oceanic and Atmospheric Administration under  
606 Award No. NA10OAR4310104. The Advanced Light Source as well as K.R.W. and T.N. were  
607 supported by the Director, Office of Energy Research, Office of Basic Energy Sciences, of the  
608 U.S. Department of Energy under Contract No. DE-AC02-05CH11231. Measurements at the  
609 Advanced Light Source were also supported by the Laboratory Directed Research and  
610 Development Program of Lawrence Berkeley National Laboratory under U.S. Department of  
611 Energy Contract No. DE-AC02-05CH11231. Caldecott tunnel measurements were supported by  
612 EPA grant RD834553. The US Environmental Protection Agency through its Office of Research  
613 and Development funded and collaborated in the research described here under Contract EP-D-  
614 10-070 to Alion Science and Technology. The manuscript has not been subjected to external peer  
615 review and has not yet been cleared for publication. Mention of trade names or commercial  
616 products does not constitute endorsement or recommendation for use. The authors would like to  
617 thank Patrick Hayes, Jose Jimenez and Sally Newman for use of AMS OA and temperature data.

618

#### 619 **References**

- 620 Borbon, A. et al. (2012), Emission ratios of anthropogenic VOC in northern mid-latitude  
621 megacities: observations vs. emission inventories in Los Angeles and Paris, *J. Geophys.*  
622 *Res.*, doi:10.1029/2012JD018235.
- 623 Dallmann, T. R., S. J. Demartini, T. Kirchstetter, S. C. Herndon, T. Onasch, E. C. Wood, and R.  
624 A. Harley (2012), On-Road Measurement of Gas and Particle Phase Pollutant Emission  
625 Factors for Individual Heavy-Duty Diesel Trucks, *Environ. Sci. Technol.*, *46*(15), 8511–  
626 8518.
- 627 Van Deursen, M., J. Beens, J. Reijenga, P. Lipman, and C. Cramers (2000), Group-Type  
628 Identification of Oil Samples Using Comprehensive Two- Dimensional Gas  
629 Chromatography Coupled to a Time-of-Flight Mass Spectrometer (GCxGC-TOF), *J. High*  
630 *Resol. Chromatogr.*, *23*, 507–510.
- 631 Frysinger, G. S., R. B. Gaines, L. Xu, and C. M. Reddy (2003), Resolving the unresolved  
632 complex mixture in petroleum-contaminated sediments., *Environ. Sci. Technol.*, *37*(8),  
633 1653–1662.
- 634 Gary, J. H., G. E. Handwerk, and M. J. Kaiser (2007), *Petroleum Refining: Technology and*  
635 *Economics*, 5th ed., Taylor and Francis, Boca Raton.
- 636 Gentner, D. R. et al. (2012), Elucidating secondary organic aerosol from diesel and gasoline  
637 vehicles through detailed characterization of organic carbon emissions, *P. Natl. Acad. Sci.*  
638 *USA*, *109*(45), 18318–18323, doi:10.1073/pnas.1212272109.
- 639 Gilman, J. B. et al. (2010), Ozone variability and halogen oxidation within the Arctic and sub-  
640 Arctic springtime boundary layer, *Atmos. Chem. Phys.*, *10*(21), 10223–10236,  
641 doi:10.5194/acp-10-10223-2010.
- 642 Goldstein, A. H., and I. E. Galbally (2007), Known and unexplored organic constituents in the  
643 earth's atmosphere, *Environ. Sci. Technol.*, *41*(5), 1514–1521.
- 644 Grieshop, A. P., M. A. Miracolo, N. M. Donahue, and A. L. Robinson (2009), Constraining the  
645 volatility distribution and gas-particle partitioning of combustion aerosols using isothermal  
646 dilution and thermodenuder measurements., *Environ. Sci. Technol.*, *43*(13), 4750–4756.
- 647 Heald, C. L. et al. (2011), Exploring the vertical profile of atmospheric organic aerosol:  
648 comparing 17 aircraft field campaigns with a global model, *Atmos. Chem. Phys.*, *11*(24),  
649 12673–12696, doi:10.5194/acp-11-12673-2011.
- 650 Hodzic, A., J. L. Jimenez, S. Madronich, M. R. Canagaratna, P. F. DeCarlo, L. Kleinman, and J.  
651 Fast (2010), Modeling organic aerosols in a megacity: potential contribution of semi-  
652 volatile and intermediate volatility primary organic compounds to secondary organic  
653 aerosol formation, *Atmos. Chem. Phys.*, *10*(12), 5491–5514, doi:10.5194/acp-10-5491-2010.

- 654 Isaacman, G. et al. (2012a), Improved resolution of hydrocarbon structures and constitutional  
655 isomers in complex mixtures using gas chromatography-vacuum ultraviolet-mass  
656 spectrometry., *Anal. Chem.*, *84*(5), 2335–2342, doi:10.1021/ac2030464.
- 657 Isaacman, G., A. W. H. Chan, T. Nah, D. R. Worton, C. R. Ruehl, K. R. Wilson, and A. H.  
658 Goldstein (2012b), Heterogeneous OH oxidation of motor oil particles causes selective  
659 depletion of branched and less cyclic hydrocarbons, *Environ. Sci. Technol.*, *46*, 10632–  
660 10640.
- 661 Isaacman, G., D. R. Worton, N. M. Kreisberg, C. J. Hennigan, A. P. Teng, S. V. Hering, A. L.  
662 Robinson, N. M. Donahue, and A. H. Goldstein (2011), Understanding evolution of product  
663 composition and volatility distribution through in-situ GC × GC analysis: a case study of  
664 longifolene ozonolysis, *Atmos. Chem. Phys.*, *11*(11), 5335–5346, doi:10.5194/acp-11-5335-  
665 2011.
- 666 Jimenez, J. L. et al. (2009), Evolution of organic aerosols in the atmosphere., *Science*,  
667 *326*(5959), 1525–1529, doi:10.1126/science.1180353.
- 668 Jordan, C. E., P. J. Ziemann, R. J. Griffin, Y. B. Lim, R. Atkinson, and J. Arey (2008), Modeling  
669 SOA formation from OH reactions with C8–C17 n-alkanes, *Atmos. Env.*, *42*(34), 8015–  
670 8026, doi:10.1016/j.atmosenv.2008.06.017.
- 671 Kwok, E. S. C., and R. Atkinson (1995), Estimation of hydroxyl radical reaction rate constants  
672 for gas-phase organic compounds using a structure-reactivity relationship: an update,  
673 *Atmos. Env.*, *29*(14), 1685–1695.
- 674 Lambe, A. T., M. A. Miracolo, C. J. Hennigan, A. L. Robinson, and N. M. Donahue (2009),  
675 Effective Rate Constants and Uptake Organic Molecular Markers in Motor Oil and Diesel  
676 Primary Radicals, *Environ. Sci. Technol.*, *43*(23), 8794–8800.
- 677 Lim, Y. B., and P. J. Ziemann (2009), Effects of molecular structure on aerosol yields from OH  
678 radical-initiated reactions of linear, branched, and cyclic alkanes in the presence of NO<sub>x</sub>,  
679 *Environ. Sci. Technol.*, *43*(7), 2328–2334.
- 680 Liu, S. et al. (2012), Secondary organic aerosol formation from fossil fuel sources contribute  
681 majority of summertime organic mass at Bakersfield, *J. Geophys. Res.*, *117*, D00V26,  
682 doi:10.1029/2012JD018170.
- 683 Mao, D., H. Van De Weghe, R. Lookman, G. Vanermen, N. De Brucker, and L. Diels (2009),  
684 Resolving the unresolved complex mixture in motor oils using high-performance liquid  
685 chromatography followed by comprehensive two-dimensional gas chromatography, *Fuel*,  
686 *88*(2), 312–318, doi:10.1016/j.fuel.2008.08.021.
- 687 Marzi, R., B. E. Torkelson, and R. K. Olson (1993), A revised carbon preference index, *Org.*  
688 *Geochem.*, *20*(8), 1303–1306.

- 689 Nelson, R. K., B. M. Kile, D. L. Plata, S. P. Sylva, L. Xu, C. M. Reddy, R. B. Gaines, G. S.  
690 Frysinger, and S. E. Reichenbach (2006), Tracking the Weathering of an Oil Spill with  
691 Comprehensive Two-Dimensional Gas Chromatography, *Environ. Forensics*, 7(1), 33–44,  
692 doi:10.1080/15275920500506758.
- 693 Pankow, J., and W. Asher (2008), SIMPOL. 1: a simple group contribution method for  
694 predicting vapor pressures and enthalpies of vaporization of multifunctional organic  
695 compounds, *Atmos. Chem. Phys.*, 8, 2773–2796, doi:10.5194/acp-8-2773-2008.
- 696 Parrish, D. D., A. Stohl, C. Forster, E. L. Atlas, D. R. Blake, P. D. Goldan, W. C. Kuster, and J.  
697 A. de Gouw (2007), Effects of mixing on evolution of hydrocarbon ratios in the  
698 troposphere, *J. Geophys. Res.*, 112(D10S34), D10S34, doi:10.1029/2006JD007583.
- 699 Pollack, I. B. et al. (2012), Airborne and ground-based observations of a weekend effect in  
700 ozone, precursors, and oxidation products in the California South Coast Air Basin, *J.*  
701 *Geophys. Res.*, 117, D00V05, doi:10.1029/2011JD016772.
- 702 Presto, A. A., C. J. Hennigan, N. T. Nguyen, and A. L. Robinson (2012), Determination of  
703 Volatility Distributions of Primary Organic Aerosol Emissions from Internal Combustion  
704 Engines Using Thermal Desorption Gas Chromatography Mass Spectrometry, *Aerosol Sci.*  
705 *Techn.*, 46(10), 1129–1139, doi:10.1080/02786826.2012.700430.
- 706 Presto, A. A., M. A. Miracolo, N. M. Donahue, and A. L. Robinson (2010), Secondary organic  
707 aerosol formation from high-NO<sub>x</sub> photo-oxidation of low volatility precursors: n-alkanes,  
708 *Environ. Sci. Technol.*, 44, 2029–2034.
- 709 Pye, H. O. T., and J. H. Seinfeld (2010), A global perspective on aerosol from low-volatility  
710 organic compounds, *Atmos. Chem. Phys.*, 10(9), 4377–4401, doi:10.5194/acp-10-4377-  
711 2010.
- 712 Robinson, A. L., N. M. Donahue, M. K. Shrivastava, E. A. Weitkamp, A. M. Sage, A. P.  
713 Grieshop, T. E. Lane, J. R. Pierce, and S. N. Pandis (2007), Rethinking organic aerosols:  
714 semivolatile emissions and photochemical aging., *Science*, 315(5816), 1259–1262,  
715 doi:10.1126/science.1133061.
- 716 Schauer, J., M. Kleeman, and G. Cass (1999), Measurement of emissions from air pollution  
717 sources. 2. C1 through C30 organic compounds from medium duty diesel trucks, *Environ.*  
718 *Sci. Technol.*, 33(10), 1578–1587.
- 719 Schauer, J., M. Kleeman, and G. Cass (2002), Measurement of emissions from air pollution  
720 sources. 5. C1-C32 organic compounds from gasoline-powered motor vehicles, *Environ.*  
721 *Sci. Technol.*, 36, 1169–1180.
- 722 Tkacik, D. S., A. A. Presto, N. M. Donahue, and A. L. Robinson (2012), Secondary organic  
723 aerosol formation from intermediate-volatility organic compounds: cyclic, linear, and  
724 branched alkanes., *Environ. Sci. Technol.*, 46(16), 8773–8781, doi:10.1021/es301112c.

- 725 Ventura, G. T., F. Kenig, C. M. Reddy, G. S. Frysinger, R. K. Nelson, B. Van Mooy, and R. B.  
726 Gaines (2008), Analysis of unresolved complex mixtures of hydrocarbons extracted from  
727 Late Archean sediments by comprehensive two-dimensional gas chromatography  
728 (GC×GC), *Org. Geochem.*, *39*(7), 846–867, doi:10.1016/j.orggeochem.2008.03.006.
- 729 Vogt, L., T. Gröger, and R. Zimmermann (2007), Automated compound classification for  
730 ambient aerosol sample separations using comprehensive two-dimensional gas  
731 chromatography-time-of-flight mass spectrometry., *J. Chromatogr. A*, *1150*(1-2), 2–12,  
732 doi:10.1016/j.chroma.2007.03.006.
- 733 Wang, F. C.-Y., K. Qian, and L. A. Green (2005), GCxMS of diesel: a two-dimensional  
734 separation approach., *Anal. Chem.*, *77*(9), 2777–2785, doi:10.1021/ac0401624.
- 735 Williams, B. J., A. H. Goldstein, N. M. Kreisberg, and S. V Hering (2010a), In situ  
736 measurements of gas/particle-phase transitions for atmospheric semivolatile organic  
737 compounds., *P. Natl. Acad. Sci. USA*, *107*(15), 6676–6681, doi:10.1073/pnas.0911858107.
- 738 Williams, B. J., A. H. Goldstein, N. M. Kreisberg, S. V. Hering, D. R. Worsnop, I. M. Ulbrich,  
739 K. S. Docherty, and J. L. Jimenez (2010b), Major components of atmospheric organic  
740 aerosol in southern California as determined by hourly measurements of source marker  
741 compounds, *Atmos. Chem. Phys.*, *10*(23), 11577–11603, doi:10.5194/acp-10-11577-2010.
- 742 Worton, D. R., N. M. Kreisberg, G. Isaacman, A. P. Teng, C. McNeish, T. Górecki, S. V.  
743 Hering, and A. H. Goldstein (2012), Thermal Desorption Comprehensive Two-Dimensional  
744 Gas Chromatography: An Improved Instrument for In-Situ Speciated Measurements of  
745 Organic Aerosols, *Aerosol Sci. Tech.*, *46*(4), 380–393, doi:10.1080/02786826.2011.634452.
- 746 Zhang, Q. et al. (2007), Ubiquity and dominance of oxygenated species in organic aerosols in  
747 anthropogenically-influenced Northern Hemisphere midlatitudes, *Geophys. Res. Lett.*, *34*,  
748 L13801, doi:10.1029/2007GL029979.
- 749 Zhao, Y. et al. (2012), Major components of summer-time organic aerosol in Bakersfield, CA, *J.*  
750 *Geophys. Res.*, submitted.

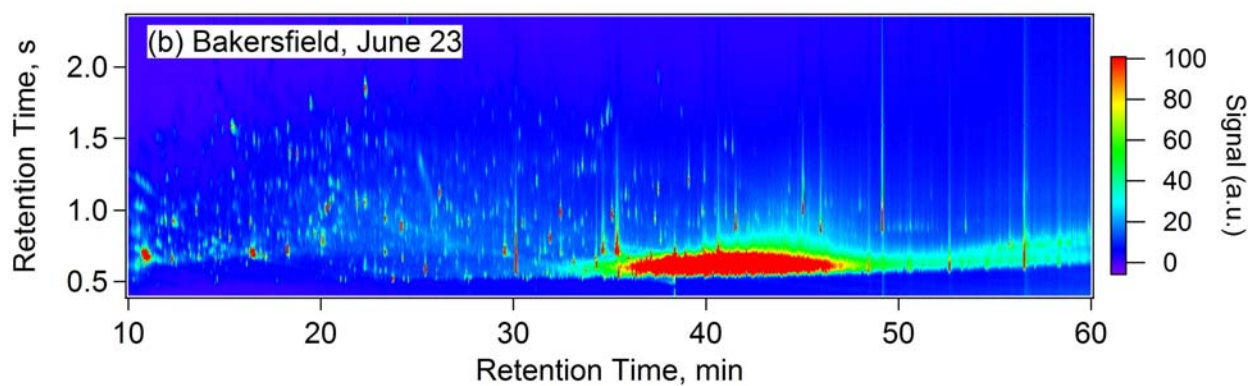
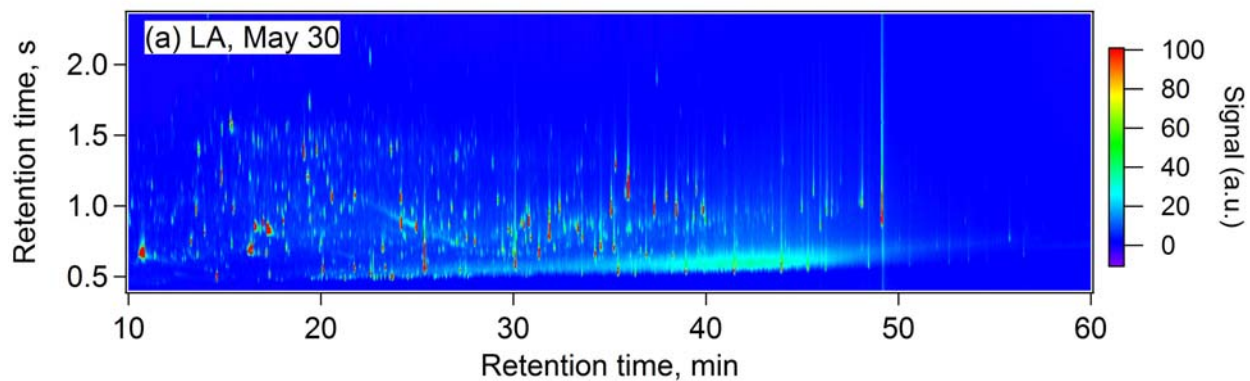
751

752 **Table 1.** Gas-phase OH reaction rate constants of linear ( $k_N$ ) and branched ( $k_B$ ) alkanes  
 753 calculated by structure-reactivity relationships (SRR) [Kwok and Atkinson, 1995], the rate ratios  
 754 ( $k_B/k_N$ ) calculated from SRR and observed in ambient LA samples. The uncertainties in observed  
 755 rate ratios are derived from the standard deviations in the regressions shown in Fig. 5. See  
 756 Appendix C in the Supplementary Material for derivation of  $k_{B1}$  from EI data.

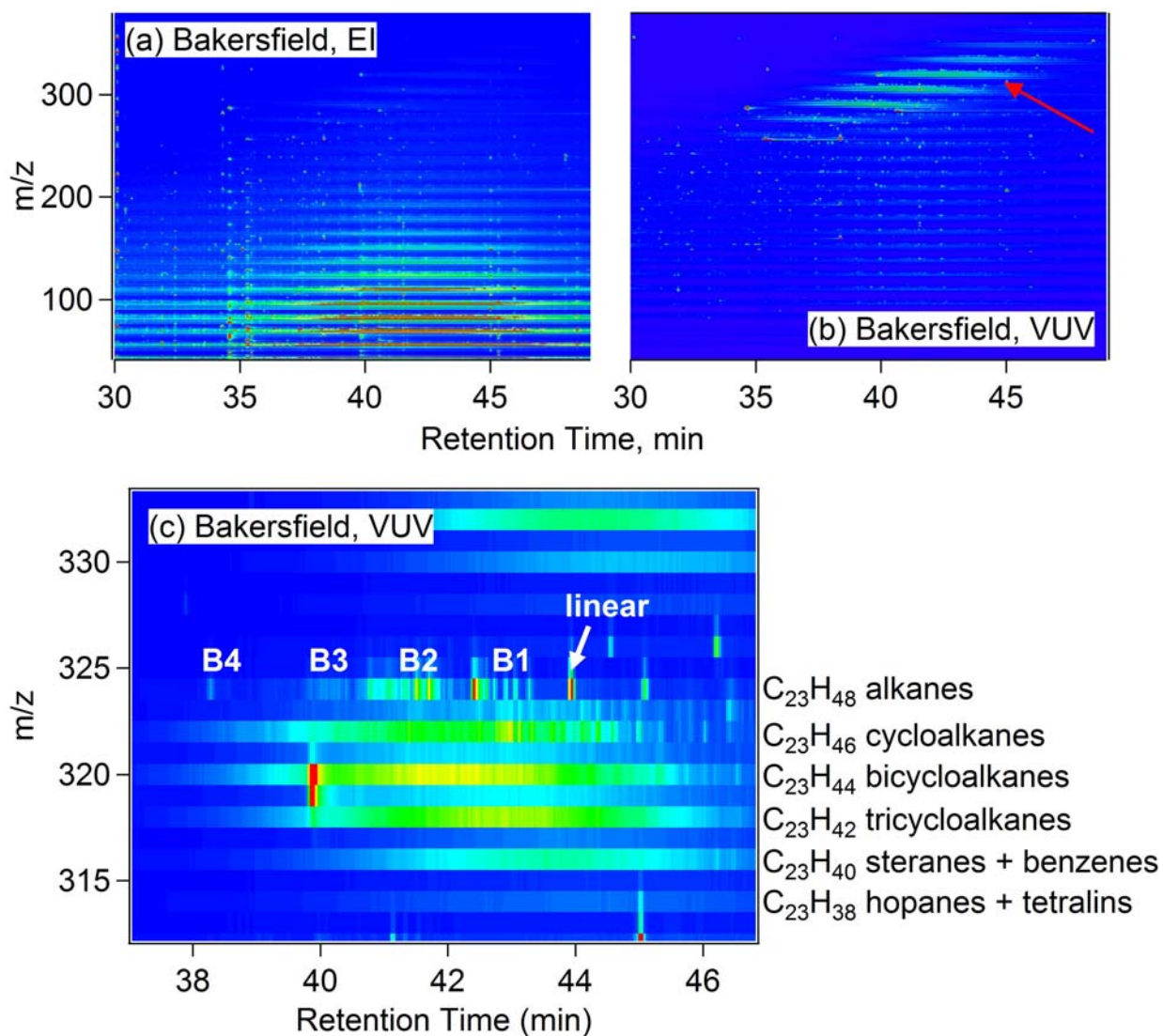
757

Carbon Number	$k_N$ ( $10^{-11}$ cm <sup>3</sup> molec <sup>-1</sup> sec <sup>-1</sup> ) from SRR	$k_B$ ( $10^{-11}$ cm <sup>3</sup> molec <sup>-1</sup> sec <sup>-1</sup> ) from SRR	$k_{B1}/k_N$ (SRR)	$k_{B2}/k_N$ (SRR)	$k_B/k_N$ observed (from VUV data)	$k_{B1}/k_N$ observed (from EI data)
21	2.66	2.88	1.08	1.01	1.21 ± 0.47	
22	2.80	3.03	1.08	1.01	1.31 ± 0.48	1.32
23	2.94	3.17	1.08	1.01	1.25 ± 0.13	1.12
24	3.08	3.31	1.07	1.01	1.35 ± 0.50	1.14

758



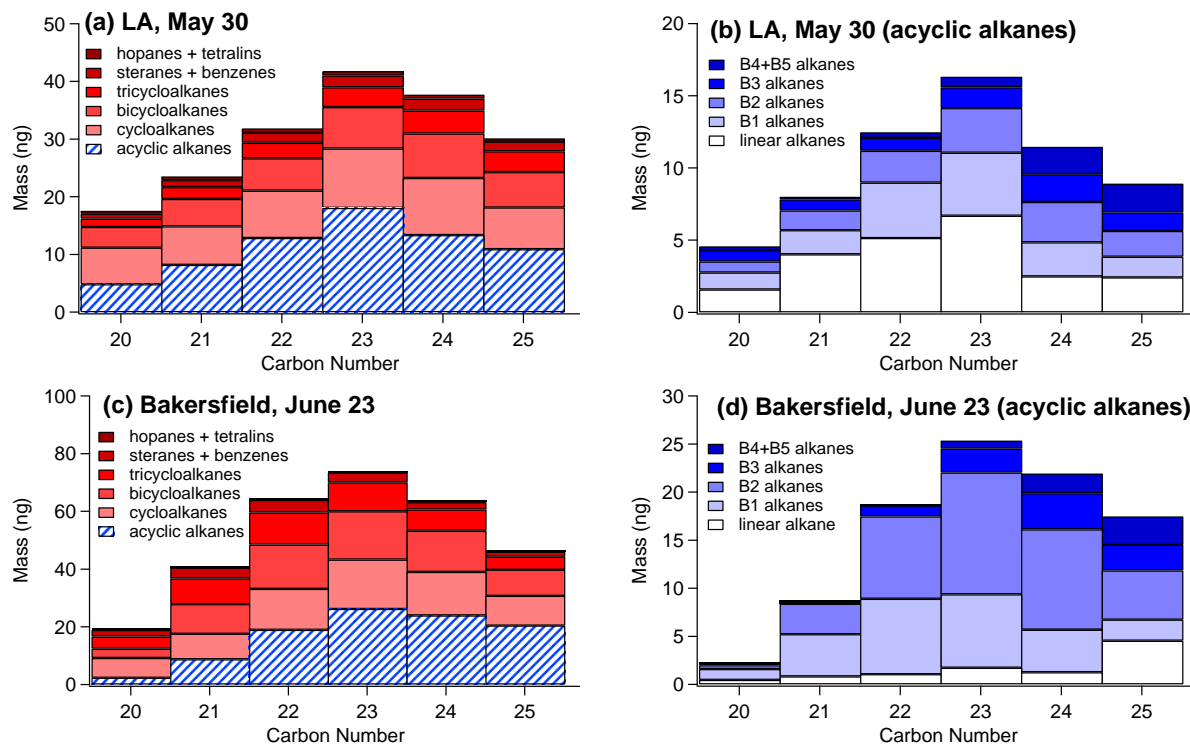
761 **Figure 1.** Total Ion Chromatogram of (a) LA sample (May 30) and (b) Bakersfield sample (June  
762 23). The unresolved complex mixture (UCM) of aliphatic hydrocarbons, between first-dimension  
763 retention times of 30 and 50 minutes, is evident in both samples.



764

765

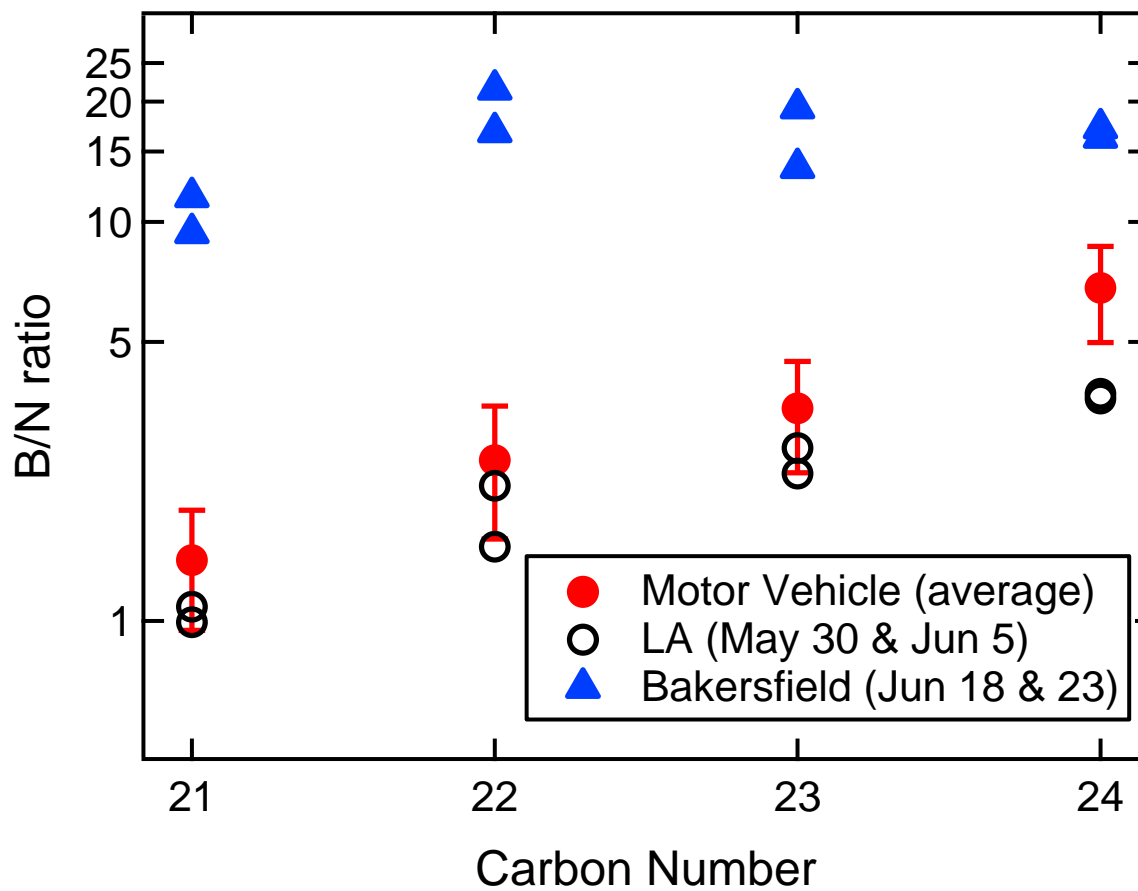
766 **Figure 2.** GCxMS plots of UCM in Bakersfield sample (June 23) under (a) EI and (b) VUV  
 767 ionization. (a) Under electron impact, strong fragmentation causes most of the signal to fall on  
 768 the same fragment  $C_xH_y^+$  ions, as delineated by horizontal lines along a few select  $m/z$ 's. (b)  
 769 Under VUV, molecular ions are retained, and cluster by carbon number in a GCxMS plot. One  
 770 such cluster denoted by the red arrow is expanded into Panel (c). Within each carbon number,  
 771 aliphatic hydrocarbons were resolved by number of rings (by molecular weight) and by degree of  
 772 branching for acyclic alkanes, denoted by  $B_x$ , where  $x$  is the number of alkyl branches.



773

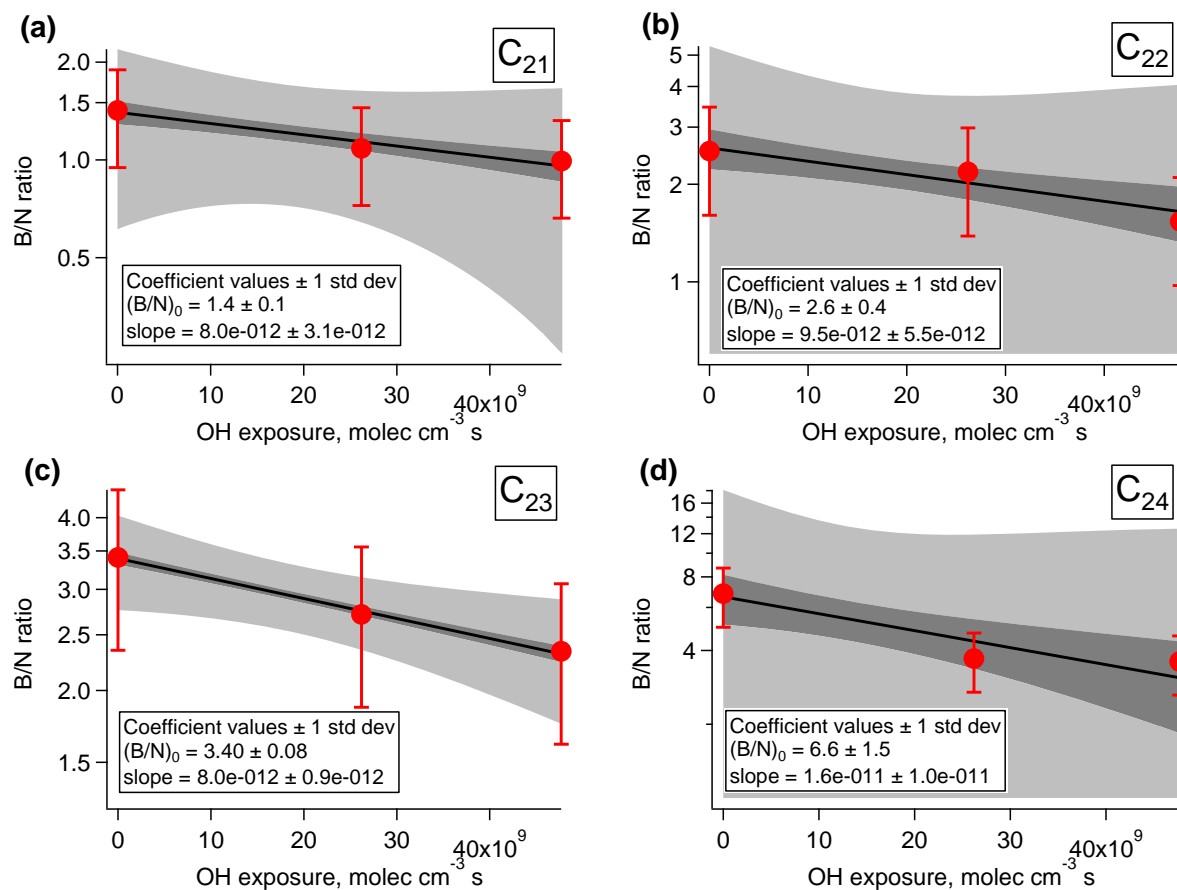
774

775 **Figure 3.** Distribution of alkane isomers in LA (May 30) and Bakersfield (June 23) samples. In  
 776 panels (a) and (c), isomers are grouped by  $N_{DBE}$ , ranging from 0 (acyclic) to 6 (hopanes and  
 777 tetralins). In panels (b) and (d), the signals include only those of acyclic (linear and branched)  
 778 alkanes. While the distributions among different  $N_{DBE}$  in LA and Bakersfield are similar, the  
 779 branched acyclic alkanes are more abundant relative to linear alkanes in Bakersfield than in LA.



780

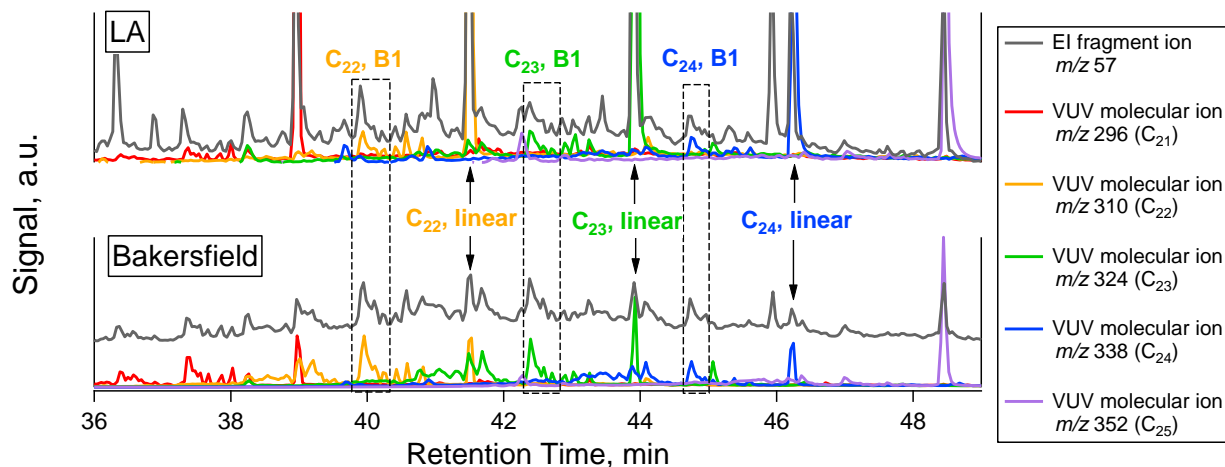
781 **Figure 4.** Ratios of branched to linear alkanes (B/N) of CalNex ambient samples and Caldecott  
 782 tunnel samples (“Motor Vehicle”) analyzed using VUV photoionization. For the motor vehicle  
 783 samples, the B/N ratios shown here averaged over all 7 samples, and the error bars represent the  
 784 standard deviations in the 7 samples.



785

786

787 **Figure 5.** Ratios of branched to linear alkanes (B/N) of LA samples measured by VUV as a  
 788 function of OH exposure. The B/N ratios at zero OH exposure are taken to be those from the  
 789 tunnel samples of fresh motor vehicle exhaust. OH exposure for the LA samples were calculated  
 790 using the ratio of 1,2,4-TMB to benzene [Borbon *et al.*, 2012]. The black lines represent the best-  
 791 fit lines to equation (1), and the fitted coefficients are shown in Table 1. The dark grey and light  
 792 grey shaded areas represent the 68% and 95% confidence intervals of the regressions,  
 793 respectively.



794

795 **Figure 6.** Extracted ion chromatograms of  $m/z$  57 under EI (dark grey) and molecular ions of

796 alkanes under VUV (all other colors). For each molecular ion, the latest eluting peak represents

797 the linear alkane. Under EI,  $m/z$  57 represents the  $C_4H_9^+$  ion, the most abundant fragment ion of

798 high molecular weight alkanes. The EI  $m/z$  57 trace show identical peak shapes to the molecular

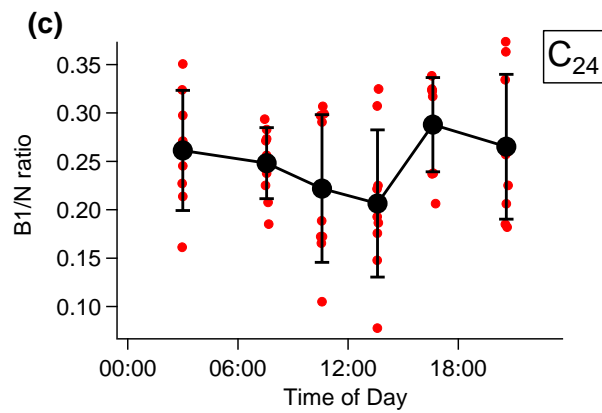
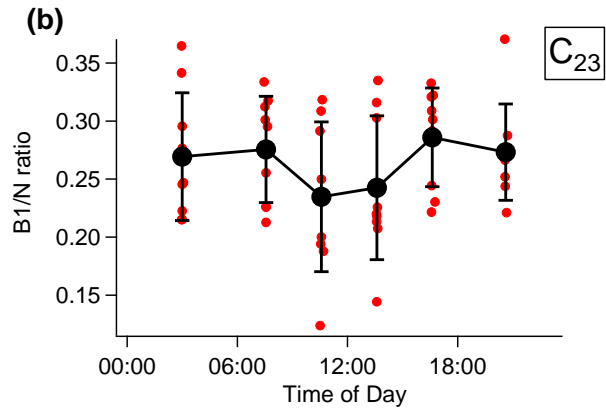
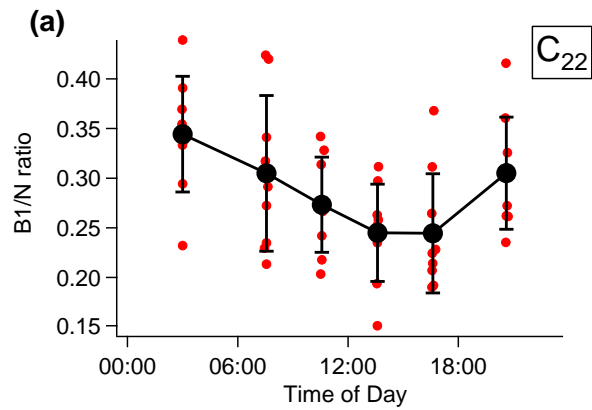
799 ion traces where the B1 isomers elute (denoted by boxes with dashed lines). Linear isomers

800 (denoted by arrows) coelute with a B2 isomer of a higher carbon number, but for  $C_{23}$ – $C_{24}$  in

801 Bakersfield samples, and  $C_{22}$ – $C_{24}$  in the LA samples, the contributions of B2 isomers are

802 expected to be less than 15%. The ratio of B1 to linear isomers (B1/N) for each carbon number

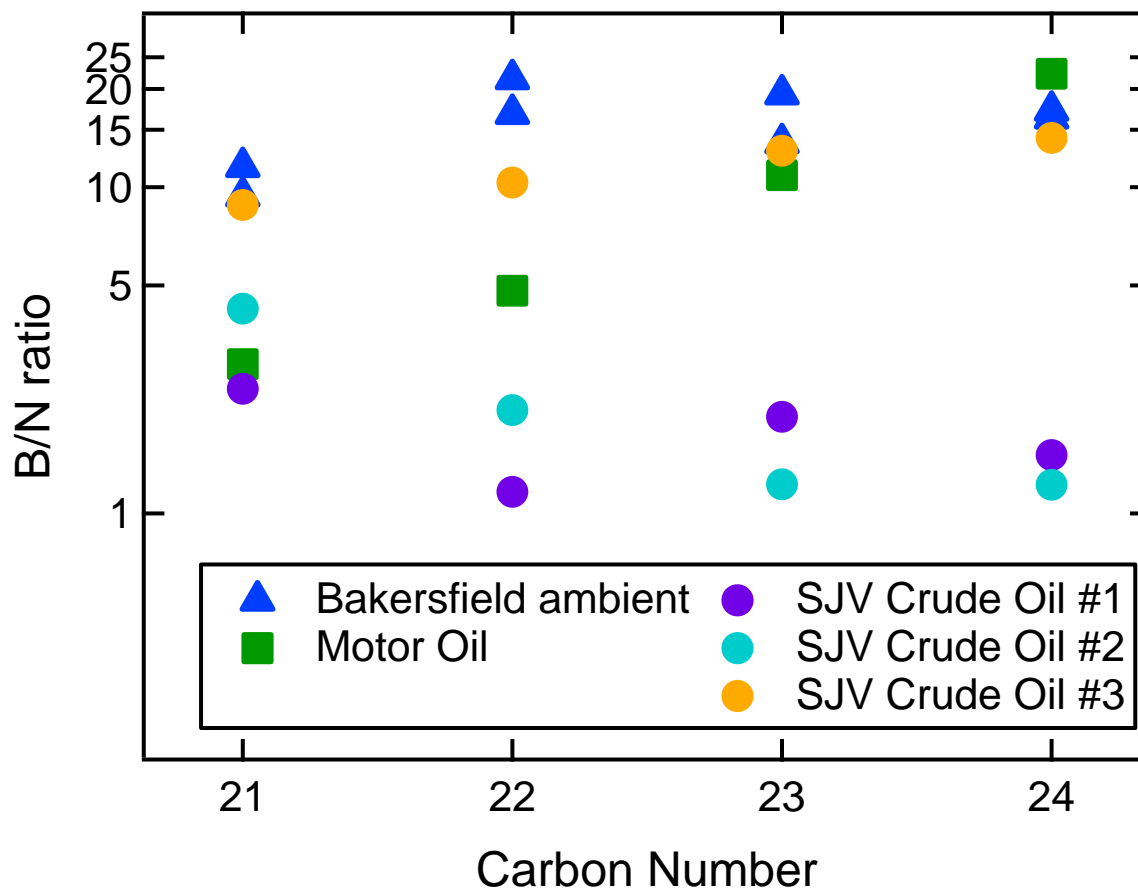
803 can therefore be estimated from the  $m/z$  57 signal under EI.



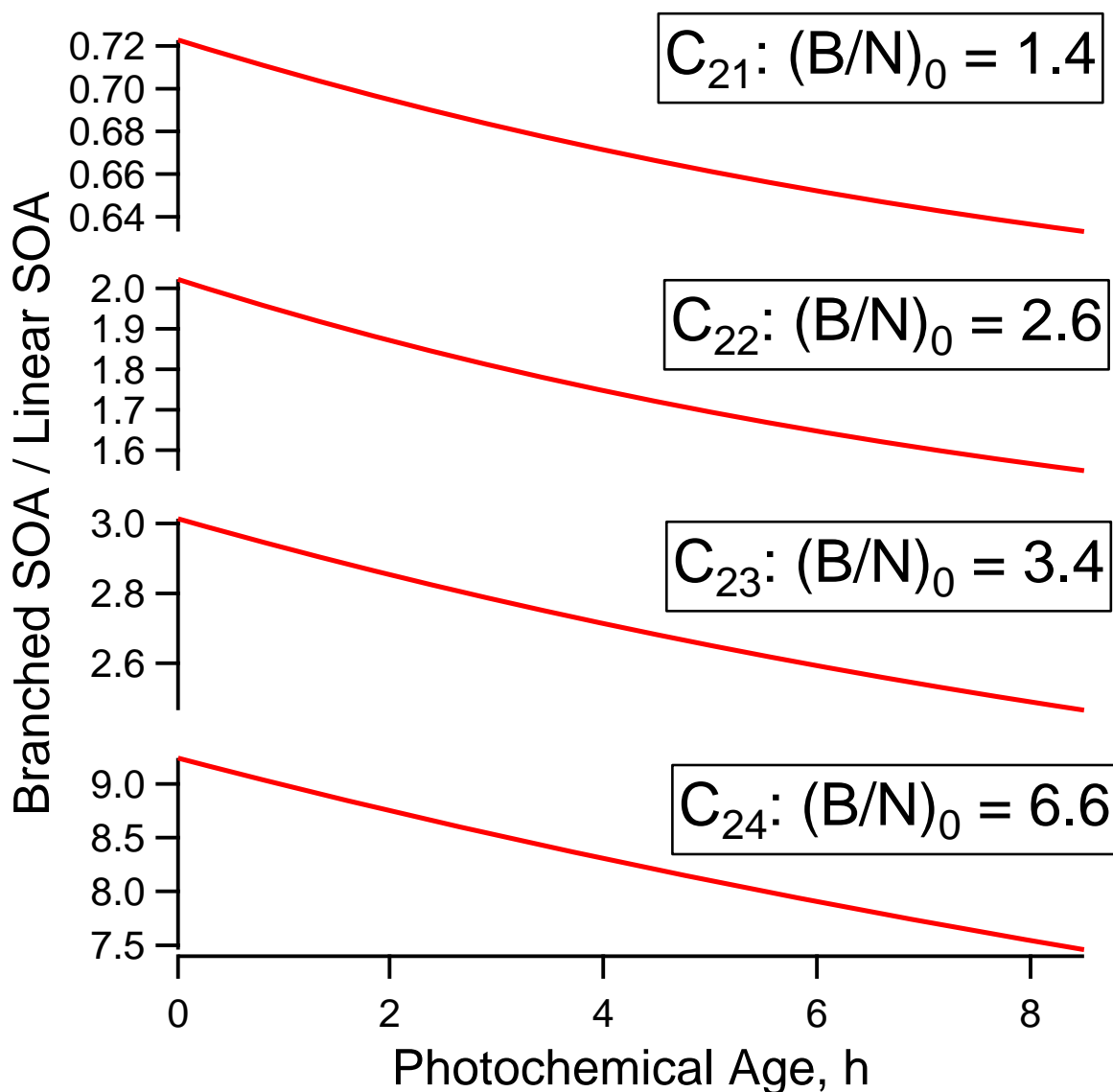
804

805

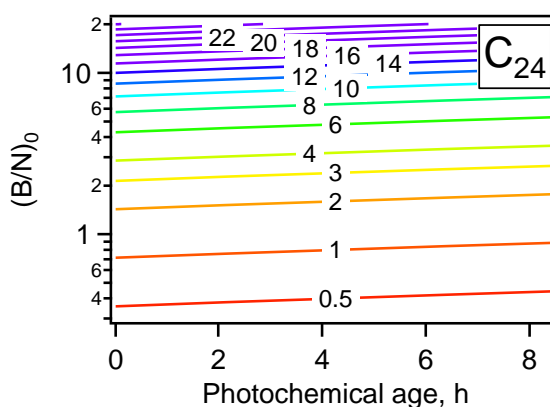
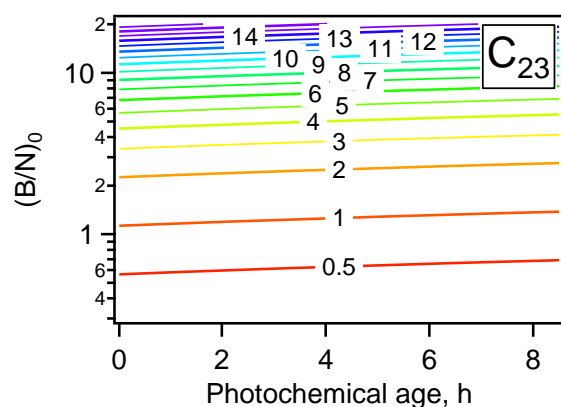
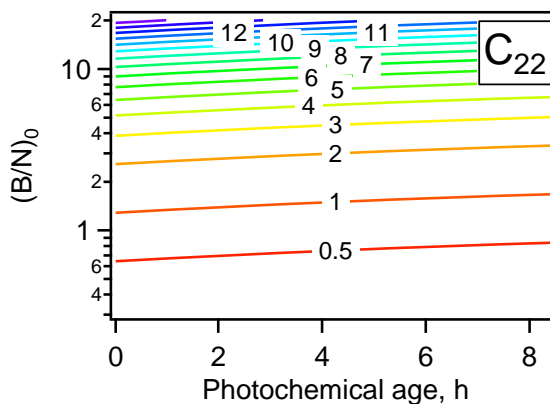
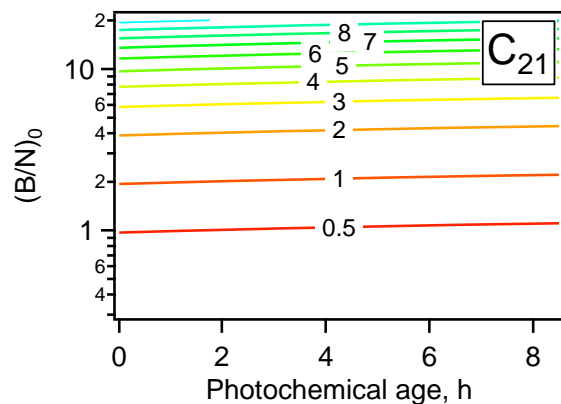
806 **Figure 7.** Diurnal profiles of B1/N ratios. The minima of B1/N ratios occur between late  
 807 morning and early afternoon local time, consistent with maximum photochemical activity.



808  
 809 **Figure 8.** Ratios of branched to linear alkanes (B/N) of ambient Bakersfield samples, 10W-30  
 810 motor oil and 3 samples of crude oil extracted and/or processed in the San Joaquin Valley (SJV).  
 811 Among all the samples analyzed in this work, the B/N ratios of motor oil and one SJV crude oil  
 812 sample (sample 3) approach those in Bakersfield, suggesting the source of these hydrocarbons is  
 813 related to oil operations in the area.  
 814



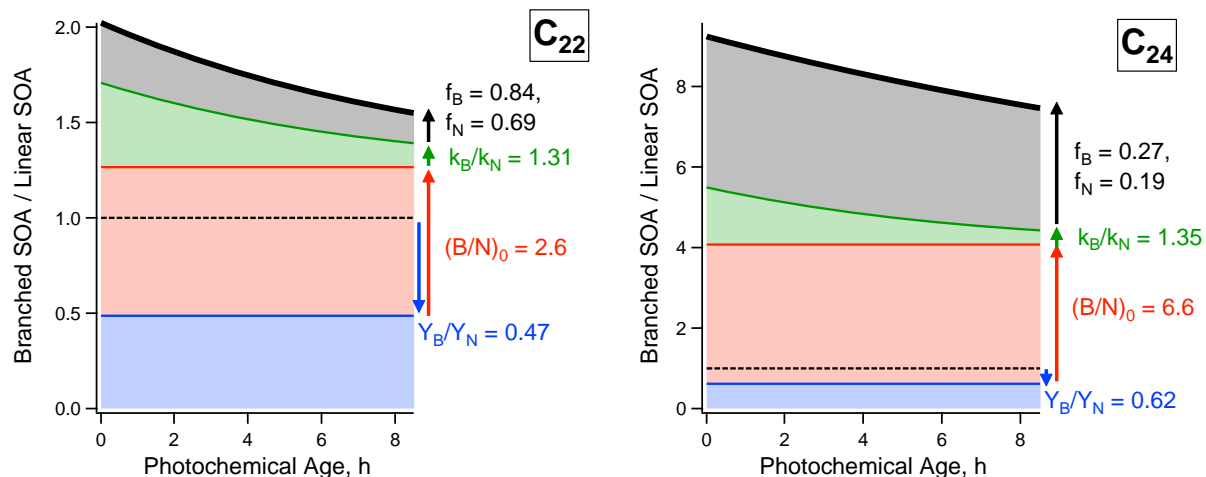
815  
 816 **Figure 9.** Base case simulation for simple box model. The mathematical equation is described by  
 817 Eqn (3). For this simulation, the values for  $(B/N)_0$  and  $k_B$  were derived from CalNex data  
 818 summarized in Table 1. SOA yields were calculated using the oxidation mechanism from *Jordan*  
 819 *et al.*, [2008], assuming 0.3 of reacted hydrocarbon fragments upon oxidation. The temperature  
 820 of 293K and organic loading is  $10 \mu\text{g m}^{-3}$ , which are typical of conditions during CalNex LA.  
 821  $[\text{OH}]$  is assumed to be constant at  $2 \times 10^6 \text{ molec cm}^{-3}$ .



822

823

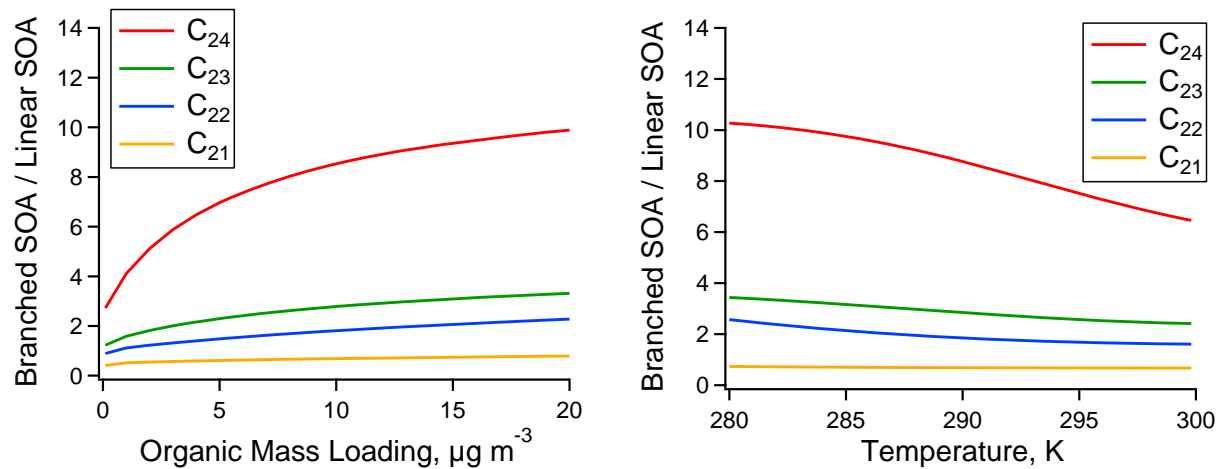
824 **Figure 10.** Contour plots of BNSOA (ratio of total SOA formation from branched alkanes to that  
 825 from linear alkanes) as a function of photochemical age and emission ratios (B/N)<sub>0</sub>. Simulations  
 826 are carried out for the range of (B/N)<sub>0</sub> observed in this work (see Figs. 4 and 8). The contour  
 827 lines are almost horizontal, indicating a stronger dependence on (B/N)<sub>0</sub> than on photochemical  
 828 age. This is a result of the linear dependence of BNSOA on (B/N)<sub>0</sub> (see Eqn (3)) and wide range  
 829 of (B/N)<sub>0</sub> observed.



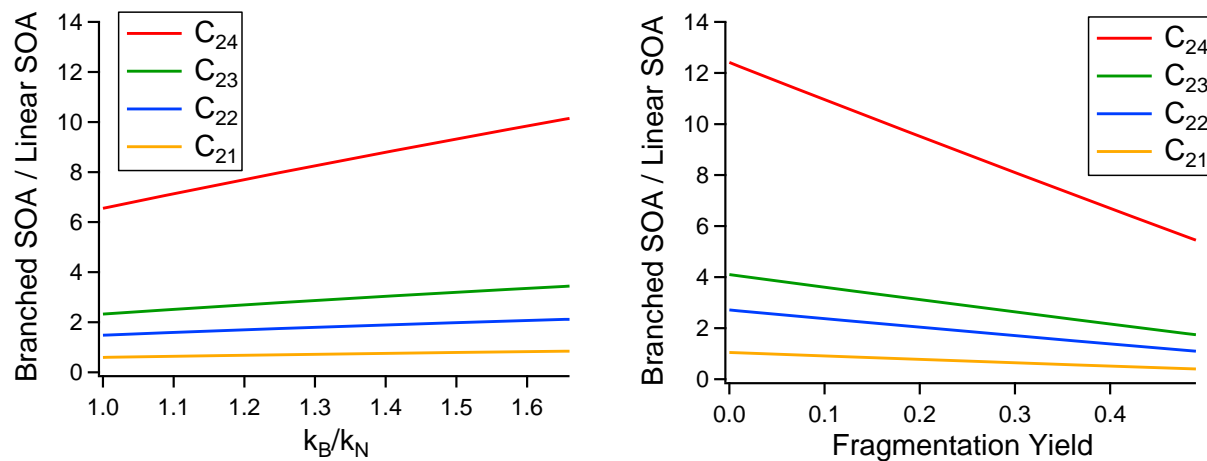
830

831 **Figure 11.** Effect of including various factors into determining relative SOA formation. The  
 832 dotted line denotes equal SOA formation between all branched isomers and the linear alkane  
 833 (BNSOA = 1). The blue line and arrow denote lowering SOA yields of branched isomers as a  
 834 result of fragmentation (0.3 in this base case). The red line and arrow denote including a higher  
 835 emission ratio of branched alkanes, derived from motor vehicle samples (see Fig. 4). The green  
 836 line and arrow denote accounting for the differences in gas-phase oxidation rate constants,  
 837 assuming all SVOCs are in the gas phase. Lastly, accounting for gas/particle partitioning results  
 838 in the black line, which represents the base case scenario. The gas phase fractions ( $f_N$  and  $f_B$ ) are  
 839 calculated for a temperature of 293K and organic loading of  $10 \mu\text{g m}^{-3}$ .

840



841  
 842 **Figure 12.** Effect of varying partitioning parameters on relative SOA formation. The range of  
 843 organic mass loading and temperature simulated here is consistent with conditions during  
 844 CalNex LA. The photochemical age for these simulations is 3 hours, at an average [OH] of  $2 \times$   
 845  $10^6$  molec cm<sup>-3</sup>. Effects of temperature on SOA yields are not taken into account, as the heat of  
 846 vaporization of oxidation products are poorly understood.  
 847



848

849 **Figure 13.** Effect of rate constants and fragmentation branching on relative SOA formation. The  
 850 fragmentation yield is molar stoichiometric yield of the fragmentation product, which is assumed  
 851 to be a ketone with half the carbon number as the parent alkane. All other parameters are kept the  
 852 same as in the base case simulation (see Fig. 9).